Temperature-dependence of impact toughness of bulk metallic glass composites containing phase transformable β-Ti crystals

Tingyi Yan [a b], Long Zhang [a c], R. Lakshmi Narayan [d], Jingyu Pang [a b], Yi Wu [a b], Huameng Fu [a c], Hong Li [a c], Haifeng Zhang [a c], Upadrasta Ramamurty [e f #]

[a] Shi-changxu Innovation Center for Advanced Materials, Institute of Metal Research, Chinese Academy of Sciences, 72 Wenhua Road, Shenyang 110016, China

[b] School of Materials Science and Engineering, University of Science and Technology of China, Shenyang 110016, China

[c] CAS Key Laboratory of Nuclear Materials and Safety Assessment, Institute of Metal Research, Chinese Academy of Sciences, Shenyang 110016, China

[d] Department of Materials Science and Engineering, Indian Institute of Technology Delhi, Hauz Khas, New Delhi 110016, India

[e] Department of Mechanical and Aerospace Engineering in Nanyang Technological University, Singapore 637331, Singapore

[f] Institute of Materials Research and Engineering, Agency for Science, Technology and Research (A ∗STAR), Singapore 138634, Singapore

Abstract

A parametric study of the Charpy impact toughness of bulk metallic glass composites (BMGCs) containing crystalline β-Ti dendrites is conducted at different temperatures. The effect of mole fractions, size and phase transformability of the dendrites in the BMGCs on impact toughness, a_K, is studied. BMGCs with non-transformable dendrites exhibit a steep drop in a_K with decreasing temperatures whereas those with transformable dendrites resist embrittlement. This is attributed to the energy absorbed during deformation-induced martensitic transformation (DIMT) in the dendrites of the phase transformable BMGC. At a specific temperature, increasing the mole fraction of phase transformable β-Ti crystals up to 70% also improves a_K, although further increase in mole fraction to 100% leads to embrittlement. The non-monotonic variation of a_K is attributed to the relative differences in confinement of the dendrite by the matrix, which directly influences the occurrence of DIMT in the former. These BMGCs are also resistant to relaxation induced embrittlement as a_K is insensitive to the casting size. The implications of these results in terms of designing BMGCs with high impact toughness for applications at low temperatures are discussed.

Graphical abstract

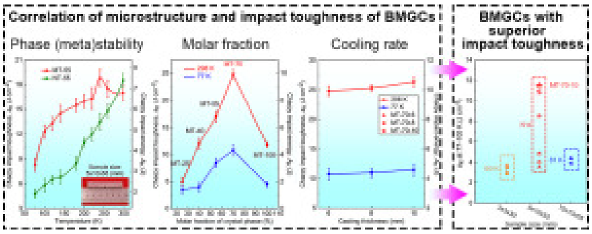

1. Download: Download high-res image (200KB)
2. Download: Download full-size image

Keywords

Bulk metallic glass composites; Charpy impact toughness; Deformation-induced martensitic transformation; Low-temperature toughening

1. Introduction

Bulk metallic glasses (BMGs) possess an excellent suite of mechanical properties such as high strength and elastic limit well below their glass transition temperature, T_g (~ 600 K for Ti- or Zr-based BMGs), but generally exhibit nil tensile ductility [1], [2], [3]. This is because their plasticity is mediated by shear bands [1,[4], [5], [6], [7], [8]], which propagate unhindered, owing to the absence of a microstructure that could interact with (and consequently hinder) them, and cause failure [1,3,4,[9], [10], [11], [12], [13]]. To enhance ductility of BMGs, the composite route, wherein a crystalline phase is incorporated into the BMG matrix to form BMG composites (BMGCs), is widely explored [14], [15], [16], [17], [18], [19], [20]. The explicit purpose of incorporating second phases is to promote the proliferation of shear bands and resist their rapid propagation. Amongst the wide variety of BMGCs, Zr/Ti-based BMGCs with body centered cubic (bcc) β-Ti/Zr dendrites [14,15,[21], [22], [23], [24], [25]] are attractive, as they exhibit a great combination of strength and ductility in addition to having good glass forming ability and processability [26], [27], [28], [29], [30], [31], [32]. In fact, recent studies show that the strength and ductility of these BMGCs can be optimized to the desired extent by changing the size, volume fraction, and phase transformability of the β-Ti crystals [30,33,34]. The resultant BMGCs also exhibit excellent room temperature (RT) mode I and mode II fracture toughness, K_Q, which is a critical parameter in the context of structural applications [29,30].

Besides ductility and the quasi-static fracture toughness, an engineering property that is important in structural applications—especially in the context of damage tolerance–is impact toughness, a_K, which is a measure of the energy absorbed by the material during impact. While 'reasonably tough' BMGs have high a_K at RT, it drops precipitously at lower temperatures [27,[35], [36], [37], [38]], which often occurs with a sharp ductile-to-brittle transition (DBT), reminiscent of that observed in bcc crystalline alloys [35,39,40]. For instance, a_K of a Zr-based BMG (Vit.1) decreases from 7.6 J cm^{-2} at 300 K to 3.4 J cm^{-2} at 100 K [27]. DBT in BMGs is an outcome of the steep rise in the stress required to operate shear transformation zones (STZs), which are unit plasticity carriers in BMGs, at lower temperatures [35]. The increase in stress to operate the STZ dramatically reduces the number of STZ transformations, which in turn, reduces the number of shear bands formed in the material during impact testing. As shear bands mediate plastic flow and hence absorb impact energy, their inability to form leads to embrittlement of BMGs.

A much more distinct DBT was observed in a Zr-based BMGC (DH3) with β-Zr(Ti) dendrites, where the a_K reduces from 29.6 to 3.6 J cm^{-2}, when the temperature is reduced from RT to 100 K [27]. One reason attributed to the sharper DBT in the case of BMGCs is that the β-Zr(Ti) dendrite reinforcements, which absorb energy via plastic deformation at RT, also undergo a DBT. The simultaneous embrittlement of the β-Zr(Ti) dendrites and BMG matrix leads a steep reduction in a_K from that at RT [27].

Recent studies have shown that phase transformable β-Ti dendrite-reinforced BMGCs exhibit significant plastic deformation and undergo strain hardening at RT as well as at lower temperatures [33,[41], [42], [43]]. In light of this development, we identify the following few issues pertaining to impact toughness and DBT in BMGCs that contain transforming and non-transforming crystalline dendrite phases.

- The ability of phase transformable β-Ti dendrites to undergo deformation-induced martensitic transformation (DIMT) at RT and lower temperatures should also facilitate energy absorption of the BMGC during impact testing. However, the BMG matrix will still undergo embrittlement at lower temperatures. Therefore, it needs to be ascertained if the deformability of β-Ti at lower temperatures will compensate for the embrittlement of the matrix and lead to a more gradual reduction of aK with decreasing temperatures instead of appearing as distinct DBT.
- It was mentioned earlier that the strain hardening behavior and extent of DIMT of the β-Ti dendrites depends on microstructural parameters such as their size and volume fraction [33]. Then, it is worth examining if these microstructural parameters also influence aK and if so, what would be their relative influence at different temperatures.
- It was found that large castings of BMGCs with non-transformable β-Ti have a considerably lower quasi-static fracture toughness (KQ) compared to smaller castings due to the differences in their cooling rates [29]. This is because large castings cool at a slower rate, which leads to structural relaxation and loss of excess free volume associated with STZs. The lack of transformable STZs also limits the formation of shear bands, which in turn, leads to embrittlement of the BMG matrix and the BMGC too. Whether a similar embrittling effect will be observed for larger castings in the case of BMGCs with phase transformable β-Ti dendrites remains to be seen.

With the motivation to address these issues, we conduct Charpy impact toughness tests on non-transformable and transformable β-Ti BMGCs at different temperatures. The effects of phase stability, mole fraction and size of β-Ti crystals on a_K of BMGCs at temperatures in the range of 77–298 K are investigated. The impact tests are supplemented by microstructural and fractographic observations of the specimens tested in different conditions. Results show that while a_K drops steeply with decreasing temperature in non-transformable β-Ti reinforced BMGCs, that of phase transformable β-Ti crystals is more gradual in the same temperature range. Also, a_K exhibits non-monotonic variations with increasing mole fraction of phase transformable β-Ti crystals. Finally, it was observed that the a_K of phase transformable BMGCs increases with increasing casting size, implying that they are resistant to relaxation-induced brittleness. The conclusions of this study serve as a critical assessment of BMGCs as a potential material for applications at low temperatures.

2. Experimental

2.1. Materials and nomenclature

Several Ti-based BMGCs were produced by arc melting mixtures of high-purity Ti, Zr, Cu, Be and Fe metals (purities over 99.8 wt.%) under a Ti-gettered high-purity argon atmosphere (Hotstar arc melter). The ingots were re-melted four times to ensure chemical homogeneity. Then, the alloys were re-arc melted in high-purity argon atmosphere and poured into a copper mold (Edmund Bühler arc melter) to produce the large-sized alloy plates with the dimensions of 6 mm (thickness) × 12 mm (width) × 60 mm (length). These BMGCs are named according to the deformation type and the designed mole fraction of the β-Ti crystals. For instance, the BMGCs in this study with nominal compositions (in at.%) of $Ti_{46.9}Zr_{33.1}Cu_{5.7}Fe_2Be_{12.3}$ and $Ti_{47.8}Zr_{33.8}Cu_{5.8}Be_{12.6}$ are referred to as NT-55 and MT-55, respectively. This is because they contain non-transformable and phase transformable (that undergo DIMT during impact loading) β-Ti crystals, respectively, both with a designed mole fraction of 55%. The prefixes "NT" and "MT" are abbreviations of “non-transforming” and “martensitic transformation”, respectively, and the subsequent number (in percentage) is the molar fraction of the β-Ti crystals in respective BMGCs.

On the basis of two-phase quasi-equilibrium solidification processing of these kind of BMGCs [23], a series of BMGCs with different predetermined mole fractions of β-Ti crystals, referred as MT-*X*, were also designed. The compositions of the MT-*X* BMGCs are $Ti_{31.1+30.4x}Zr_{31+5.1x}Cu_{10-7.6x}Be_{27.9-27.9x}$ (at.%), where $x = X/100$ is the designed mole fraction of the β-Ti dendrites that ranges from 0.25 to 1.00, with an interval of 0.15. The volume fraction, x', of the dendrites can be estimated using the relation: $x'=x/[x + 0.834(1-x)]$ [23]. Plates with a thickness of 6 mm of the MT-*X* BMGCs were prepared by using the above-mentioned method. In addition, plates with the thickness of 8 and 10 mm of the MT-70 BMGC were also processed, which together with its 6 mm-thick plate are labeled as MT-70–6, MT-70–8 and MT-70–10, respectively. For quick reference, the abbreviated names and the compositions of all the investigated BMGCs are listed in Table 1.

Table 1. The compositions and abbreviated names of the investigated BMGCs. The measured volume fraction, $V_β$, average crystal size of β-Ti, and the EDS-determined compositions of both phases are also listed.

BMGCs	**Compositions (at.%)**	**$V_β$ (%)**	**β-Ti size (µm)**	**Elemental content* (at.%)**				
Empty Cell	Empty Cell	Empty Cell	Empty Cell	**Phase**	**Ti (±1.4)**	**Zr (±1.3)**	**Cu (±0.6)**	**Fe (±0.4)**
NT-55	$Ti_{46.9}Zr_{33.1}Cu_{5.7}Fe_2Be_{12.3}$	60.3 ±1.8	3.6 ±1.2	β-Ti glass	60.2 42.1	34.1 43.9	3.9 10.9	1.8 3.1
MT-25	$Ti_{38.7}Zr_{32.3}Cu_{8.1}Be_{20.9}$	29.4 ±1.6	0.5 ±0.3	β-Ti glass	60.7 43.4	36.7 42.7	2.6 13.9	0 0
MT-40	$Ti_{43.2}Zr_{33.1}Cu_7Be_{16.7}$	44.6 ±2.2	1.8 ±0.9	β-Ti glass	61.1 43.5	36.6 42.5	2.3 14	0 0

BMGCs	Compositions (at.%)	V_{β} (%)	β-Ti size (µm)	Elemental content* (at.%)				
Empty Cell	Empty Cell	Empty Cell	Empty Cell	**Phase**	**Ti (±1.4)**	**Zr (±1.3)**	**Cu (±0.6)**	**Fe (±0.4)**
MT-55	$Ti_{47.8}Zr_{33.8}Cu_{5.8}Be_{12.6}$	60.5 ±2.3	3.9 ±1.3	β-Ti glass	61.4 43.4	36.1 42.9	2.5 13.7	0 0
MT-70–6	$Ti_{52.3}Zr_{34.6}Cu_{4.7}Be_{8.4}$	74.0 ±1.8	7.2 ±1.9	β-Ti glass	61.9 42.6	35.9 43.5	2.2 13.9	0 0
MT-70–8	$Ti_{52.3}Zr_{34.6}Cu_{4.7}Be_{8.4}$	74.3 ±2.1	8.6 ±1.6	β-Ti glass	61.2 43.0	36.3 42.6	2.5 14.4	0 0
MT-70–10	$Ti_{52.3}Zr_{34.6}Cu_{4.7}Be_{8.4}$	73.8 ±2.5	10.1 ±1.8	β-Ti glass	61.4 43.5	36.6 43.1	2.0 13.4	0 0

*Beryllium cannot be detected by EDS, which is almost fully dissolved in glassy matrix [75].

2.2. Microstructural characterization

Specimens for microstructural characterization by means of X-ray diffraction (XRD, Philips PW 1050, Cu-*K*α) and scanning electron microscopy (SEM, Tescan Mira 3) combined with energy-dispersive X-ray spectroscopy (EDS) were cut from the as-cast plates. The volume fractions and sizes of β-Ti phases were measured using the computer software ImageJ (https://imagej.nih.gov/ij). Differential scanning calorimetry (DSC, Netzsch 204F1) was performed on BMGCs to measure the glass transition temperature (T_g), crystallization temperature (T_x), enthalpy of structural relaxation ($\Delta H_{rel.}$). For performing transmission electron microscopy (TEM, Talos F200) investigations, thin slices were cut from the as-cast BMGC plates, which were further ground and ion-milled in a liquid-nitrogen cooled Gatan 695 device. Lateral surfaces and fractured surfaces of the impact-loading tested samples were observed by SEM and laser scanning confocal microscopy (Zeiss LSM700), while further TEM characterization was performed on the specimens extracted from a region ~1.5 mm ahead of the notch tip in the impact-tested samples.

2.3. Charpy impact testing

The cast plates were cut into bar-shaped specimens with the dimensions of 5 mm (thickness) × 10 mm (width) × 55 mm (length), as per the Charpy impact toughness testing (ASTM E23–2018) [44]. Prior to testing, their surfaces were carefully ground with ultrafine sandpapers. A U-shape notch with a depth of 2 mm and a notch root radius of 1 mm was made in the middle of each specimen. Testing was performed on the Charpy impact instrument (MTS, ZBC2452-D) operating at a maximum hammer speed of 5.3 m s^{-1}. The Charpy impact energy, A_K, from it, is converted into the Charpy impact toughness, a_K, using the relation: $a_K = A_K/S_{area}$, where S_{area}=40 mm^2 is the cross-sectional area at the notched section. The temperatures for impact, which are ranged between

298 K (room temperature, RT) and 77 K (liquid nitrogen temperature) was maintained using a liquid nitrogen chamber. At least three specimens were tested for each BMGC at each testing temperature.

3. Results

3.1. Role of phase stability of crystals

The effect of phase stability of the β-Ti crystals on a_K of two $Ti_{46.9}Zr_{33.1}Cu_{5.7}Fe_2Be_{12.3}$ (at.%, NT-55) and $Ti_{47.8}Zr_{33.8}Cu_{5.8}Be_{12.6}$ (at.%, MT-55) BMGCs were first investigated. MT-55 is a recently developed BMGC, which contains the phase transformable β-Ti crystals that undergo DIMT of β-Ti ↔ α″-Ti under tension [34]. Because Fe is a strong β-Ti stabilizer [45], the β-Ti crystals in NT-55 with 2 at.% addition of Fe are expected to be stable and plastically deform via dislocation-mediated plasticity under impact loading. The XRD patterns of the as-cast NT-55 and MT-55 plates (6 mm thick) are shown in Figs. 1(a) and (b), respectively. Only the diffraction peaks of a BCC phase superimposed on diffraction of an amorphous phase can be detected in both the alloys, suggesting a dual-phase microstructure in the BMGCs. Representative SEM micrographs of the two BMGCs are shown in Figs. 1(c) and (d), respectively. Both of them show a microstructure that is typical of BMGCs with β-Ti dendrites uniformly distributed in the glassy matrix. The volume fraction and average dendritic size (secondary arm) of the β-Ti phase, listed in Table 1, are similar in the two BMGCs. However, the compositions of the β-Ti phase are different, which changes from $Ti_{60.2}Zr_{34.1}Cu_{3.9}Fe_{1.8}$ (at.%) in NT-55 to $Ti_{61.4}Zr_{36.1}Cu_{2.5}$ (at.%) in MT-55. Both Fe and Cu are β-Ti stabilizers and a decrease in their contents from NT-55 to MT-55 implies a decrease in phase stability of β-Ti. The EDS-measured compositions of the glassy matrix are also listed in Table 1. Figs. 1(e) and (f) show the TEM micrographs with insets of selected-area electron diffraction (SAED) patterns of the as-cast NT-55 and MT-55 BMGCs. Crystals embedded in a featureless matrix are observed in both the alloys, and the SAED patterns confirm the amorphous nature of the matrix and the BCC crystal structure of the β-Ti phase. However, athermal ω-Ti is also detected in the upper inset in Fig. 1(f), implying that β-Ti crystals in MT-55 are metastable in nature [46,47].

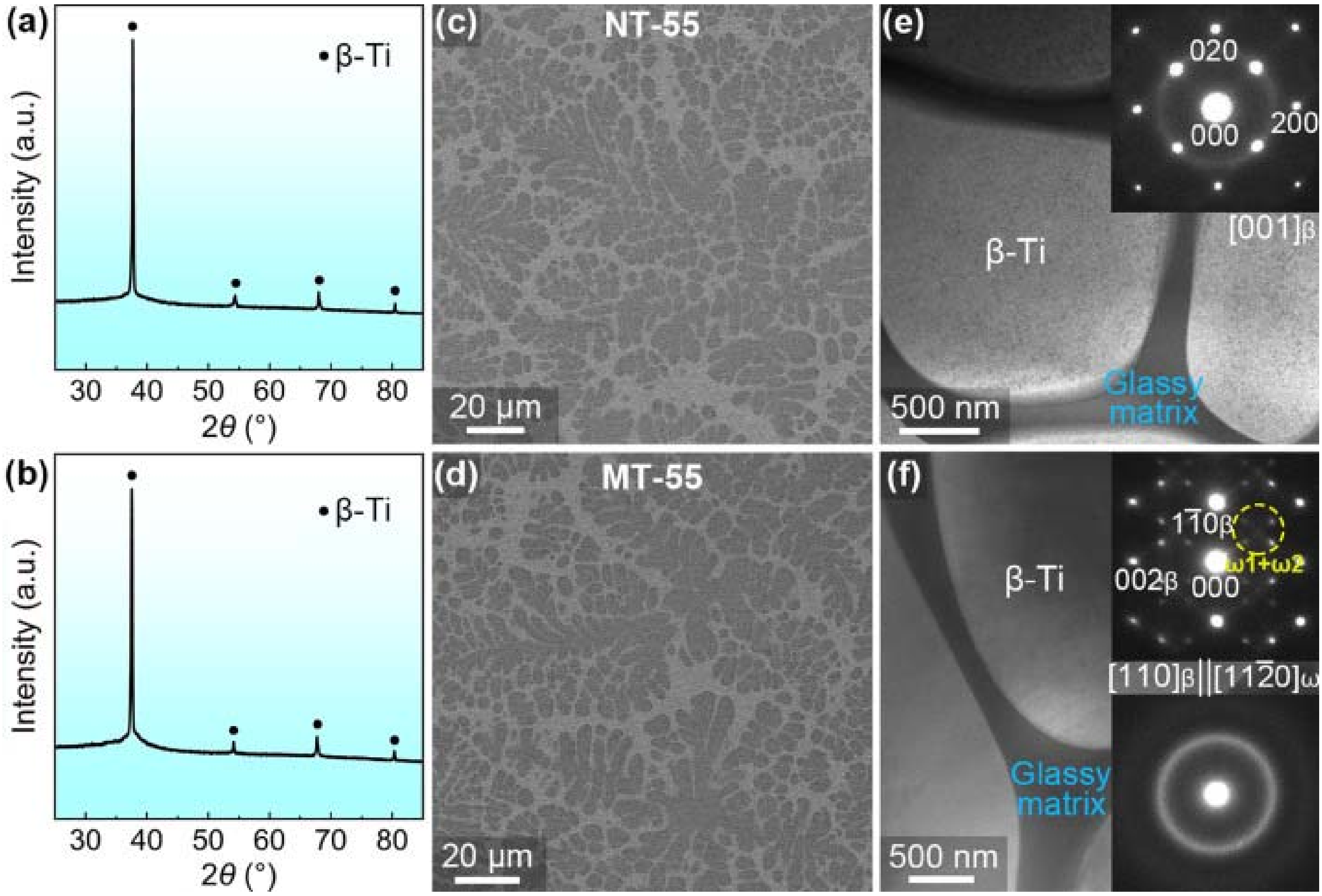

1. Download: Download high-res image (1MB)
2. Download: Download full-size image

Fig. 1. (a) and (b) XRD patterns, (c) and (d) SEM micrographs, (e) and (f) TEM micrographs with insets of SAED patterns of the as-cast NT-55 and MT-55 alloys, respectively.

Fig. 2 shows the variations of the measured a_K and A_K of the NT-55 and MT-55 at temperatures ranging from 298 K down to 77 K at 20 – 40 K intervals. The inset of Fig. 2 shows one typical image of the large-sized Charpy impact specimens used in this study. With decreasing temperature, a drastic—but monotonic—reduction in a_K of the NT-55, from 18.5 ± 0.8 J cm^{-2} at 298 K to 5.8 ± 0.8 J cm^{-2} at 100 K and 4.8 ± 0.5 J cm^{-2} at 77 K, showing considerable embrittlement at low temperatures. The variation of a_K of NT-55 with T is broadly similar to that previously-reported for Zr-based BMGCs with stable β-Zr(Ti) crystals [27,48], but no obvious DBT with a drastic drop in toughness, observed in the DH3 BMGC, can be noticed in NT-55. The contrasting trend of impact toughness variations in the two BMGCs, despite having similar volume fractions of dendrites, is attributed to compositional differences and inherent state of the amorphous matrix, which in turn influences the temperature sensitivity of stress required to activate carriers of plasticity in them [49]. Moreover, note that in the previous study [27,48], impact toughness tests on DH3 were performed on miniaturized specimens while standard impact specimens of NT-55 were used in the present study. While there is no doubt that the authors in the previous study have carefully calibrated the impact energy of miniaturized specimens, there is growing evidence that toughness in BMG and BMGCs is also sensitive to the size and geometry of the specimen [50,51]. Therefore, it is possible that the difference in the nature of the DBT of the two alloys is merely a dimension-related artefact. In contrast, a_K of MT-55 increases by ~10% from 17.0 ± 1.0 J cm^{-2} at 298 K to 18.8 ± 1.0 J cm^{-2} at 240 K, listed in Table 2. Importantly, the reduction in a_K with further decrease in T to 100 K is not as drastic as that seen in NT-55; for example, its a_K at 100 K of 12.3 ± 0.8 J cm^{-2} is more than twice that of NT-55 and more than three times that of the monolithic Vit.1 BMG (3.4 J cm^{-2}) and the DH3 BMGC (3.6 J cm^{-2} at 100 K) [27]. When T is further lowered to 77 K, a_K reduces rapidly to 8.3 ± 0.8 J cm^{-2} at 77 K, which is still 1.8 times that of NT-55, and more than twice that of the Vit.1 BMG and the DH3 BMGC.

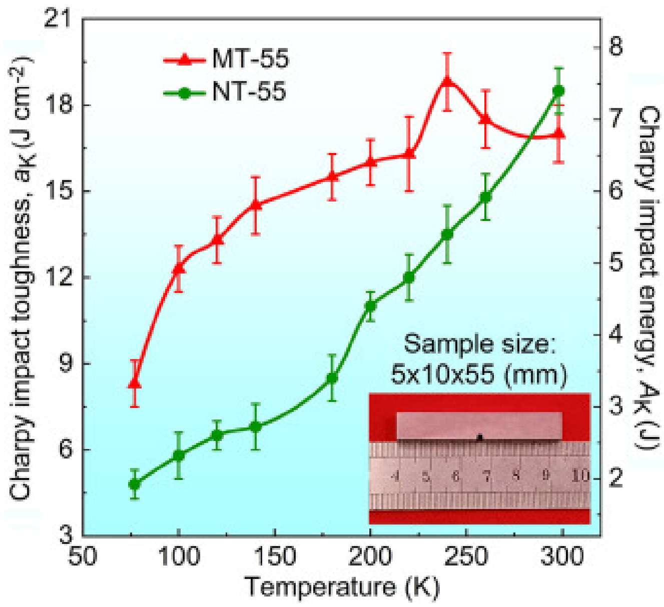

1. Download: Download high-res image (283KB)
2. Download: Download full-size image

Fig. 2. Charpy impact toughness, a_K, and impact energy, A_K, of NT-55 and MT-55 at various temperatures. The inset shows a typical image of the large-sized samples used for testing.

Table 2. Charpy impact toughness, a_K, and impact energy, A_K, of the studied BMGCs.

BMGCs	***T* (K)**	**a_K (J cm^{-2})**	**A_K (J)**
MT-25	298	5.1 ± 0.8	2.0 ± 0.3
	77	3.5 ± 0.5	1.4 ± 0.2
MT-40	298	12.0 ± 1.0	4.8 ± 0.4
	77	4.0 ± 0.8	1.6 ± 0.3

BMGCs	T (K)	a_K (J cm^{-2})	A_K (J)
MT-55	298	17.0 ± 1.0	6.8 ± 0.4
	260	17.5 ± 1.0	7.0 ± 0.4
	240	18.8 ± 1.0	7.5 ± 0.4
	220	16.3 ± 1.3	6.5 ± 0.5
	200	16.0 ± 0.8	6.4 ± 0.3
	180	15.5 ± 0.8	6.2 ± 0.3
	140	14.5 ± 1.0	5.8 ± 0.4
	120	13.3 ± 0.8	5.3 ± 0.3
	100	12.3 ± 0.8	4.9 ± 0.3
	77	8.3 ± 0.8	3.3 ± 0.3
NT-55	298	18.5 ± 0.8	7.4 ± 0.3
	260	14.8 ± 0.8	5.9 ± 0.3
	240	13.5 ± 1.0	5.4 ± 0.4
	220	12.0 ± 0.8	4.8 ± 0.3
	200	11.0 ± 0.5	4.4 ± 0.2
	180	8.5 ± 0.8	3.4 ± 0.3
	140	6.8 ± 0.8	2.7 ± 0.3
	120	6.5 ± 0.5	2.6 ± 0.2
	100	5.8 ± 0.8	2.3 ± 0.3
	77	4.8 ± 0.5	1.9 ± 0.2
MT-70–6	298	24.8 ± 0.8	9.9 ± 0.3
	77	10.8 ± 1.0	4.3 ± 0.4
MT-70–8	298	25.3 ± 0.5	10.1 ± 0.2
	77	11.0 ± 0.8	4.4 ± 0.3
MT-70–10	298	26.3 ± 0.8	10.5 ± 0.3
	77	11.5 ± 1.0	4.6 ± 0.4
MT-100	298	11.8 ± 0.6	4.7 ± 0.2
	77	4.5 ± 0.5	1.8 ± 0.2

Figs. 3(a) and (b) show the side-views of the NT-55 specimens impact tested at 298 and 77 K, respectively. Compared to the case at 77 K, the crack path in the specimen tested at 298 K is considerably more tortuous. Higher magnification images obtained from the plastically-deformed regions adjacent to the major cracks of these specimens are shown in Figs. S1(a) and (b), respectively, in the Supplementary Material. The width of the plastic regions is ~120 μm at 298 K. It decreases markedly to ~20 μm at 77 K Figs. 3.(c) and (d) show the respective SEM micrographs. Deformation bands and minor cracks, continuously penetrating both the glassy matrix and β-Ti crystals, are seen in both micrographs. However, the density of deformation bands is much higher in the specimen fractured at 298 K than that at 77 K.

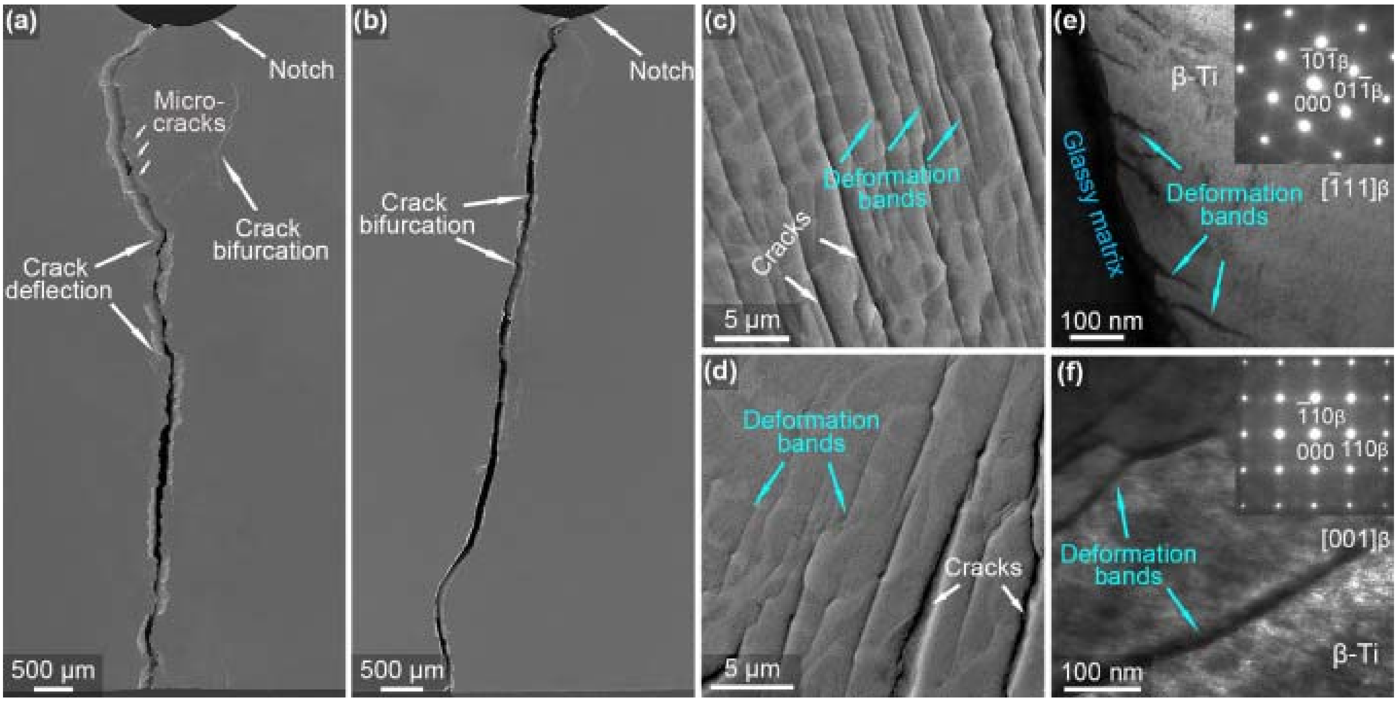

1. Download: Download high-res image (896KB)
2. Download: Download full-size image

Fig. 3. (a) and (b) Side-view of the fractured NT-55 at 298 K and 77 K, respectively. (c) and (d) SEM micrographs, (e) and (f) TEM micrographs with inset of SAED patterns of the fractured NT-55 at 298 K and 77 K, respectively.

The entire fracture surface of NT-55 tested at 298 K is shown in Fig. S2. It shows a corrugated morphology and the macroscopic roughness on the fracture surface decreases with distance away from the notch. Selected fracture morphologies of the NT-55 specimens tested at 298, 240, 140 and 77 K are shown in Fig. S3(a). Evidently, the fracture surfaces become smoother with the decreasing *T*, and the corrugations observed in the samples tested at 298 K become almost absent in the samples tested at 77 K. These observation imply a progressive reduction in the energy consumed during the fracture of NT-55 with decreasing *T*. Selected TEM micrographs of the regions close to the fracture surfaces in NT-55–6 tested at 298 and 77 K are shown in Figs. 3(e) and (f), respectively. In both the cases, deformation bands are observed in the crystalline phases, which still retain the BCC β-Ti structure, confirming that the crystals in NT-55 plastically deform without undergoing DIMT.

Figs. 4(a) and (b) show the side-views of the MT-55 specimens impact tested at 298 and 77 K, respectively. Like that seen in NT-55 case, the crack path at 298 K is again much more tortuous as compared to that at 77 K. However, the fracture paths in MT-55 are relatively more tortuous than those of NT-55 at respective temperatures. The plastically deformed regions alongside the major crack of the MT-55 specimens fractured at 298 and 77 K are also displayed in Figs. S1(c) and (d), respectively. The widths of the plastic regions adjacent to the cracks are ~90 μm at 298 K and ~30 μm at 77 K. Figs. 4(c) and (d) show the higher magnification SEM micrographs of these regions. No deformation bands or cracks are seen. Instead, many martensitic reliefs are observed inside the β-Ti crystals, while the shear bands are arrested well within the glassy ligaments. Careful examination reveals that a higher density of martensitic plates exists in the MT-55 tested at 298 K than that tested at 77 K.

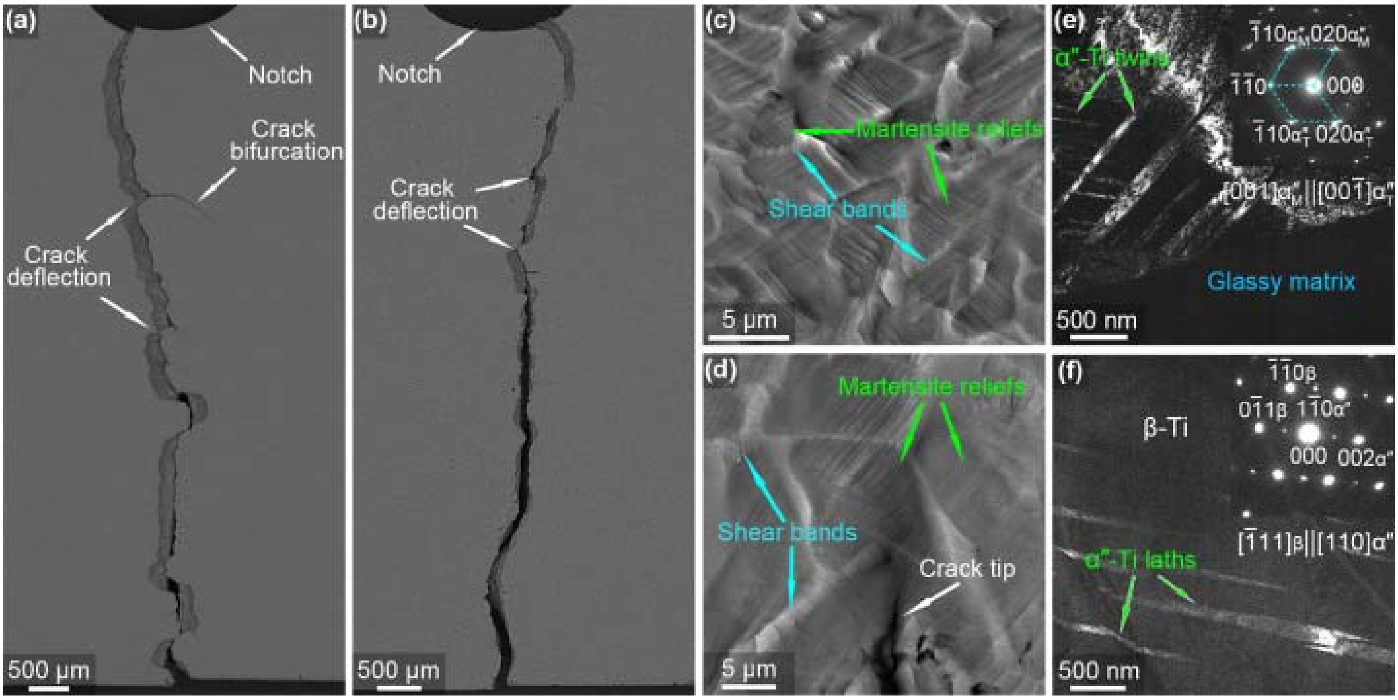

1. Download: Download high-res image (1MB)
2. Download: Download full-size image

Fig. 4. (a) and (b) Side-view of the fractured MT-55 at 298 K and 77 K, respectively. (c) and (d) SEM micrographs, (e) and (f) TEM micrographs with inset of SAED patterns of the fractured MT-55 at 298 K and 77 K, respectively.

The entire fracture surface of MT-55 tested at 298 K is displayed in Fig. S4. Similar to that of NT-55 at 298 K, the fracture surface of MT-55 also corrugated, and the macroscopic roughness gradually decreases with the distance away from the notch. For comparison, representative fracture surfaces of MT-55 specimens tested at 298, 240, 140 and 77 K are shown in Fig. S3(b). The fracture surface roughness increases as T decreases from 298 to 240 K. Further reduction in T leads to slight smoothening of the fracture surfaces. However, the fracture surface of the MT-55 specimen tested at 77 K is much rougher than that of NT-55. The TEM micrographs of MT-55 specimens tested at 298 and 77 K are displayed in Figs. 4(e) and (f), respectively. The SAED patterns (show in the insets) confirm that the martensitic phase in the fractured MT-55 specimen corresponds to the orthorhombic α″-Ti martensite. A high density of α″-Ti plates and their $\{110\}_{\alpha''}$ twins are observed in the MT-55 specimen tested at 298 K. Their fraction is smaller in the specimen tested at 77 K.

3.2. Role of fractions of crystals

The effect of phase transformable β-Ti crystalline volume fraction, x', on a_K of a series of BMGCs was investigated next. Since the cooling rate does not affect the β-Ti fraction, the MT-55 BMGC can be considered to be in a two-phase quasi-equilibrium between the supercooled liquid and the precipitated β-Ti crystals that occur during solidification [23]. Consequently, the equation given below was used to design BMGCs with a predetermined amount of x':

$$(1)\quad C_c^i=(1-x)C_M^i+xC_\beta^i,$$

where, CCi, CMi and Cβi are the concentrations of i^{th} element in the designed BMGCs, in the glassy matrix and β-Ti phase of MT-55 (which are listed in Table 1), respectively. The mole fractions of β-Ti in the BMGCs, x, are designed to be 0.25, 0.40, 0.70 or 1.00. They are referred to as MT-X (X = 100x), here afterwards Fig. 5(a) shows the XRD patterns of the MT-X BMGCs. As x increases from 0.25 to 0.70, the diffraction peaks corresponding to β-Ti become more prominent, suggesting an increase in x' in the BMGC. Additional, but less prominent, diffraction peaks are detected in the XRD pattern of MT-70, which correspond to α″-Ti. MT-100 is a fully crystalline α″-Ti alloy, suggesting the polycrystalline β-Ti phase is unstable. Microstructures of MT-25, MT-40, MT-70 and MT-100 specimens are shown in Figs. 5(b) to (e), respectively. With an increase in x, the actual volume fraction of β-Ti realized, x', increases from 29.4 ± 1.6% in MT-25 to 44.6 ± 2.2% in MT-40, 74.0 ± 1.8% in MT-70 and 100% in MT-100, respectively. Thus, the relation between x and x' obeys: $x'=x/[x + 0.834(1-x)]$. In addition, the dendritic size also increases, which are measured and listed in Table 1. The chemical compositions of the β-Ti crystals in all the MT-X BMGCs are similar to that in the MT-55 specimen, which is the outcome of the two-phase quasi-equilibrium nature [23]. Selected TEM micrographs obtained from the MT-25 and MT-70 BMGCs are shown in Figs. 5(f) and (g), respectively. While MT-25 has a microstructure of fine β-Ti single-crystals embedded in the glassy matrix, much larger crystals along with a small fraction of α″-Ti laths are observed in MT-70. The DSC scans obtained on the as-cast MT-X BMGCs are shown in Fig. S5. No obvious thermal events could be detected for MT-100, confirming its full crystalline state. All the other BMGCs exhibit a glass transition, confirming the existence of a glassy phase. The observation of a gradual decrease in the intensity of exothermic peaks of crystallizations from MT-25 to MT-70 indicates the reduction in the volume fraction of the glassy matrix.

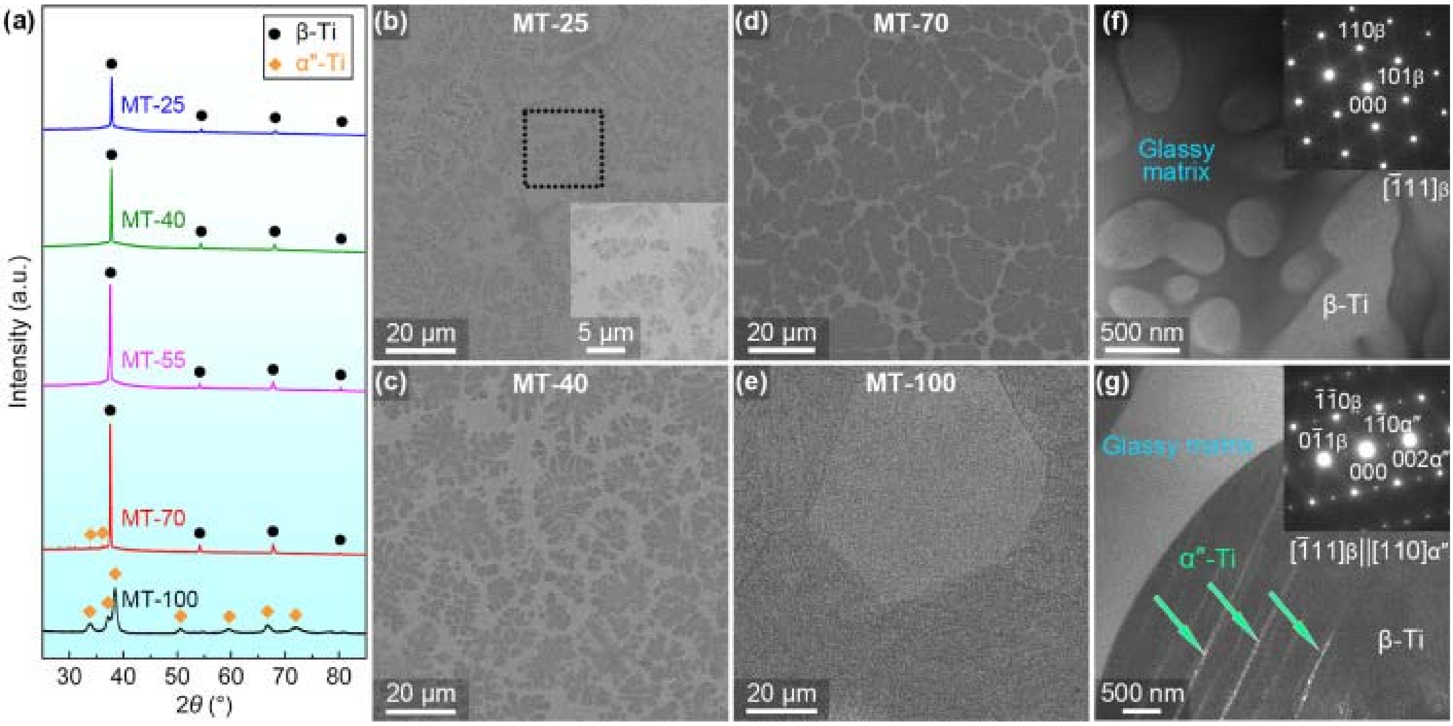

1. Download: Download high-res image (1MB)
2. Download: Download full-size image

Fig. 5. (a) XRD patterns of as-cast MT-X alloys. (b)-(e) SEM micrographs of as-cast MT-25 (with an inset of local magnified micrograph), MT-40, MT-70 and MT-100 alloys, respectively. (f) and (g) TEM micrographs of the as-cast MT-25 and MT-70 with insets of SAED patterns, respectively.

Fig. 6 shows the variations of a_K and A_K with mole fraction, x, of the MT-X BMGCs tested at 298 and 77 K. With an increase in x, a_K at 298 K initially increases from 5.1 ± 0.8 J cm^{-2} of MT-25 to 12.0 ± 1.0 of MT-40, 17.0 ± 1.0 of MT-55 and 24.8 ± 0.8 J cm^{-2} of MT-70, then decreases to only 11.8 ± 0.6 J cm^{-2} of MT-100. The a_K of the full-crystalline MT-100 at 298 K is much smaller than MT-70 and MT-55. At 77 K, a_K of MT-X exhibits a similar microstructural dependence, which firstly increases from 3.5 ± 0.5 J cm^{-2} of MT-25 to 4.0 ± 0.8 J cm^{-2} of MT-40, 8.3 ± 0.8 J cm^{-2} of MT-55, 10.8 ± 1.0 J cm^{-2} of MT-70, and then decreases to only 4.5 ± 0.5 J cm^{-2} of MT-100. It is obvious in Fig. 6 that MT-70 exhibits the highest a_K at both 298 and 77 K.

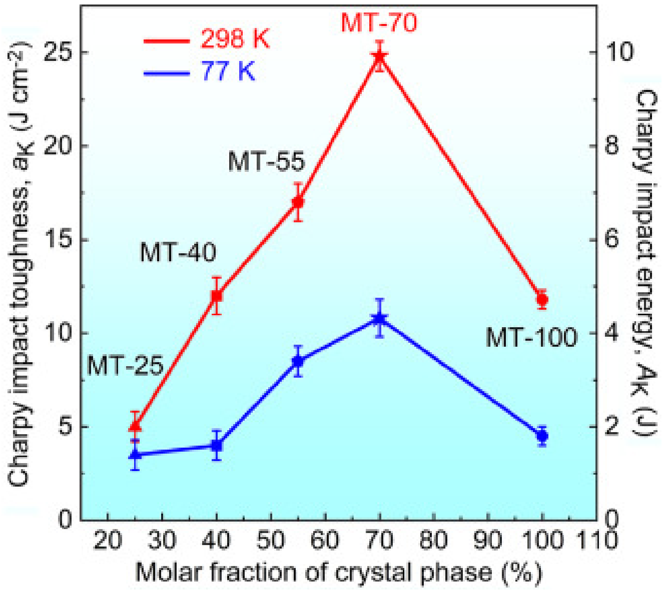

1. Download: Download high-res image (247KB)
2. Download: Download full-size image

Fig. 6. Charpy impact toughness, a_K, and impact energy, A_K, of MT-X at 298 and 77 K.

Selected images of the crack paths in the MT-25 samples fractured at 298 and 77 K are shown in Figs. 7(a) and (b), respectively. Although tortuous crack paths are observed in both the samples, it is relatively more at 298 than at 77 K. The plastically deformed regions adjacent to them are shown in Figs. S6(a) and (b), respectively. The width of the plastic regions is ~30 µm at 298 K, which decreases to ~20 µm at 77 K. Higher magnification SEM micrographs of the deformed regions in the MT-25 specimens fractured at 298 and 77 K are shown in Figs. 7(c) and (d), respectively. In both the cases, the deformation bands penetrating both the glassy matrix and β-Ti crystals can be seen, but are sparse. Several deformation bands have evolved into cracks. Fine martensitic reliefs can also be seen in the β-Ti crystals in both the samples. TEM images obtained from the deformed regions of the MT-25 samples fractured at 298 and 77 K are shown in Figs. 7(e) and (f), respectively. The observation of α″-Ti laths in the in β-Ti crystals of the specimen fractured at 298 K exist suggests that DIMT takes place during impact loading. The fraction of α″-Ti laths is lower in the sample tested at 77 K, which implies that impact loading also induces a small fraction of martensitic transformation of MT-25 at that T.

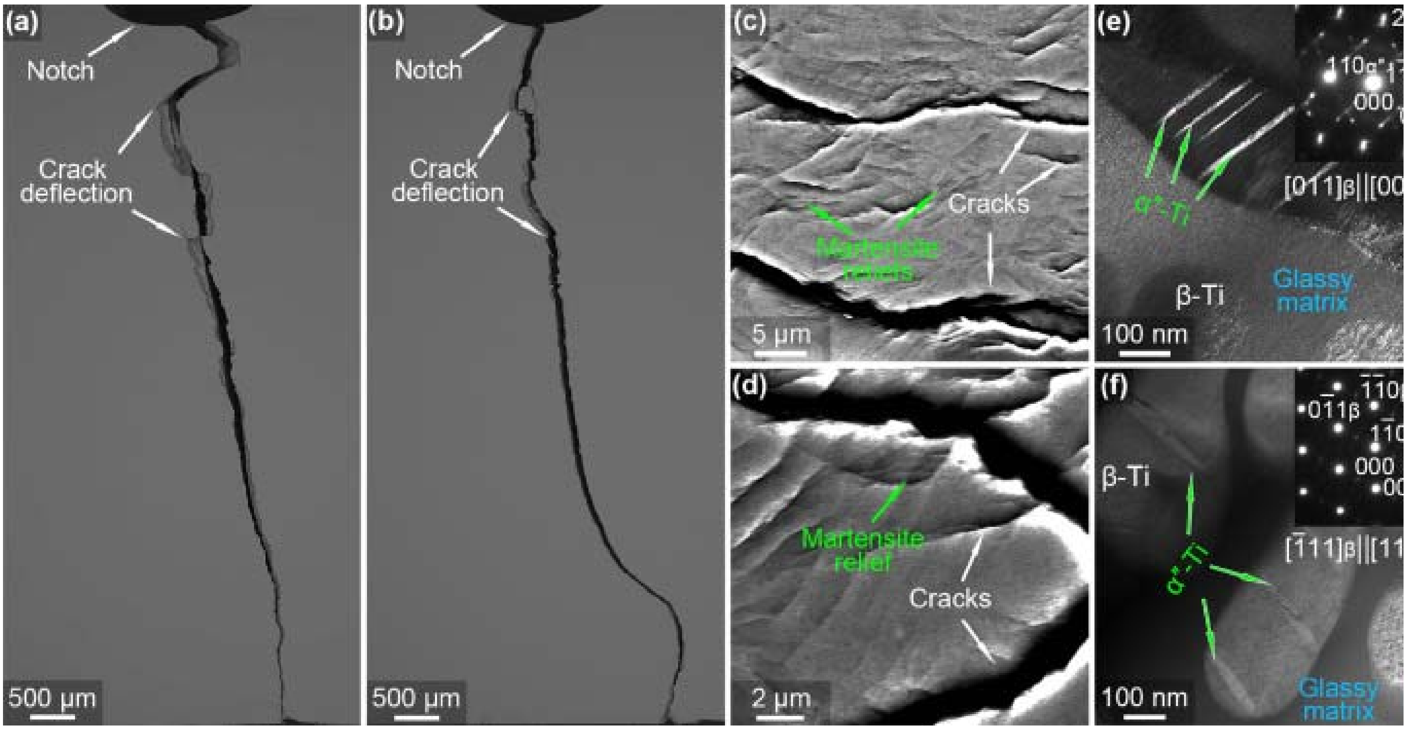

1. Download: Download high-res image (922KB)
2. Download: Download full-size image

Fig. 7. (a) and (b) Side-view of the fractured MT-25 at 298 K and 77 K, respectively. (c) and (d) SEM micrographs, (e) and (f) TEM micrographs with inset of SAED patterns of the fractured MT-25 at 298 K and 77 K, respectively.

Figs. 8(a) and (b) show the side-views of the MT-70 samples fractured at 298 and 77 K, respectively. The crack path in the MT-70 specimen tested at 298 K has many bifurcations and deflections. While similar features are also seen in the specimen tested at 77 K, the crack path is less tortuous than that at 298 K. The plastically deformed regions adjacent to the major cracks of the MT-70 specimens fractured at 298 and 77 K are displayed in Figs. S6(e) and (f), respectively. The widths of the plastic regions are ~180 μm at 298 K and ~70 μm at 77 K, respectively. Both of these are much larger than those noted in the other BMGCs at respective *T*. Figs. 8(c) and (d) show the SEM micrographs of the deformed regions. A high density of martensitic reliefs inside β-Ti crystals along with a high density of shear bands within the glassy ligaments are observed in the MT-70 specimen tested at 298 K. The density of martensitic reliefs and shear bands in the case of specimen tested at 77 K is far smaller. Figs. 8(e) and (f) show the TEM micrographs obtained from the MT-70 specimens tested at 298 and 77 K, respectively. A large number of α″-Ti martensitic plates, as confirmed by the SAED pattern, exist in the sample fractured at 298 K, implying that the β→α″ transformation occurs profusely during the impact loading of the sample. Similar α″-Ti plates, different from those observed in the as-cast state, were also observed in the specimen tested at 77 K, suggesting that DIMT also takes place at 77 K. It is noteworthy that the α″-Ti plates with a different plate orientation are observed in one β-Ti crystal, indicating that at least two α″-Ti $\{021\}_{\alpha''}$ variants form during impact loading [52,53].

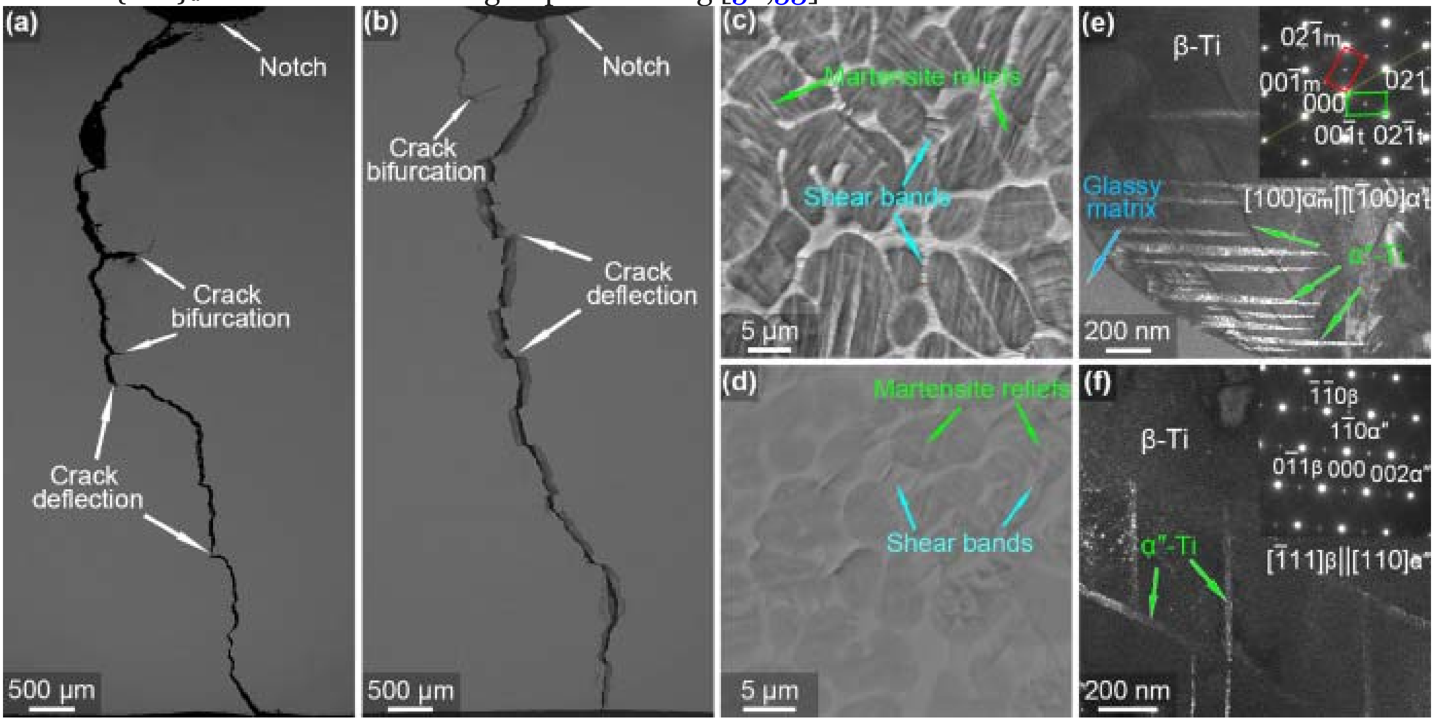

1. Download: Download high-res image (939KB)
2. Download: Download full-size image

Fig. 8. (a) and (b) Side-view of the fractured MT-70 at 298 K and 77 K, respectively. (c) and (d) SEM micrographs, (e) and (f) TEM micrographs with inset of SAED patterns of the fractured MT-70 at 298 K and 77 K, respectively.

The fracture surfaces of the MT-*X* BMGC samples tested at 298 and 77 K were also observed with the three-dimensional laser scanning confocal microscopy. Results obtained are displayed in Fig. S7. With increasing the fraction of the phase transformable β-Ti crystals, the macroscopic fracture morphologies of MT-*X* BMGCs tested at 298 K increasingly become coarser, which can be gauged by the maximum in the height difference between peak and valley positions (Fig. S7(a)). In comparison, although the height difference of the MT-*X* BMGCs tested at 77 K largely fluctuates, the fracture surfaces are getting microscopically rougher, as reflected by the local regions of ups and downs (Fig. S7(b)). Therefore, with increasing the fraction of β-Ti fractions from MT-25 to MT-70, the BMGCs exhibit much rougher facture surfaces at both 298 and 77 K.

3.3. Role of cooling rates

Since the 6 mm plates of MT-70 BMGC exhibit the highest a_K, this composition was chosen to investigate the effect of cooling rates on a_K. For this purpose, plates of MT-70 with a thickness of 8 and 10 mm were produced. An additional digit indicating the plate thickness is provided in the names of the MT-70 BMGCs, which with increasing the cast thickness are referred to as MT-70–6, MT-70–8 and MT-70–10, respectively. Prior work has shown that the cooling rate, R, is inversely proportional to the square of the smallest casting dimension, t, i.e., $R \propto (1/t^2)$ [54]. This means the cooling rates of MT-70–8 and MT-70–10 are only 56% and 36%, respectively, of MT-70–6. Fig. 9(a) shows the XRD patterns of the as-cast MT-70 plates. All the three MT-70 plates mainly exhibit diffraction peaks of β-Ti crystals superimposed on humps of the glassy matrix. However, with an increase in the plate thickness (and hence a decrease in the cooling rate), the smaller peaks of α″-Ti become more intensive, suggesting a high fraction of α″-Ti forms. This is because a lower cooling rate always favors the formation of martensitic phase within the metastable β-Ti crystals [45,55]. Figs. 9(b) and (c) show the microstructures of the MT-70–8 and MT-70–10 BMGCs, respectively. A comparison with the microstructure of the MT-70–6 BMGC displayed in Fig. 5(d) indicates that the volume fractions of β-Ti crystals remain invariant. Quantitative measurements indicate that they are 74.0 ± 1.8% in MT-70–6, 74.3 ± 2.1% in MT-70–8 and 73.8 ± 2.5% in MT-70–10. The compositions of the β-Ti crystals in MT-70–8 and MT-70–10, listed in Table 1, are also similar to that of MT-70–6. The DSC traces obtained on these three BMGCs are similar, as shown in Fig. S8. However, with a decreasing cooling rate, an increase in the average size of β-Ti crystals (secondary arms), from 7.2 ± 1.9 μm of MT-70–6 to 8.6 ± 1.6 μm of MT-70–8 and 10.1 ± 1.8 μm of MT-70–10, was noted.

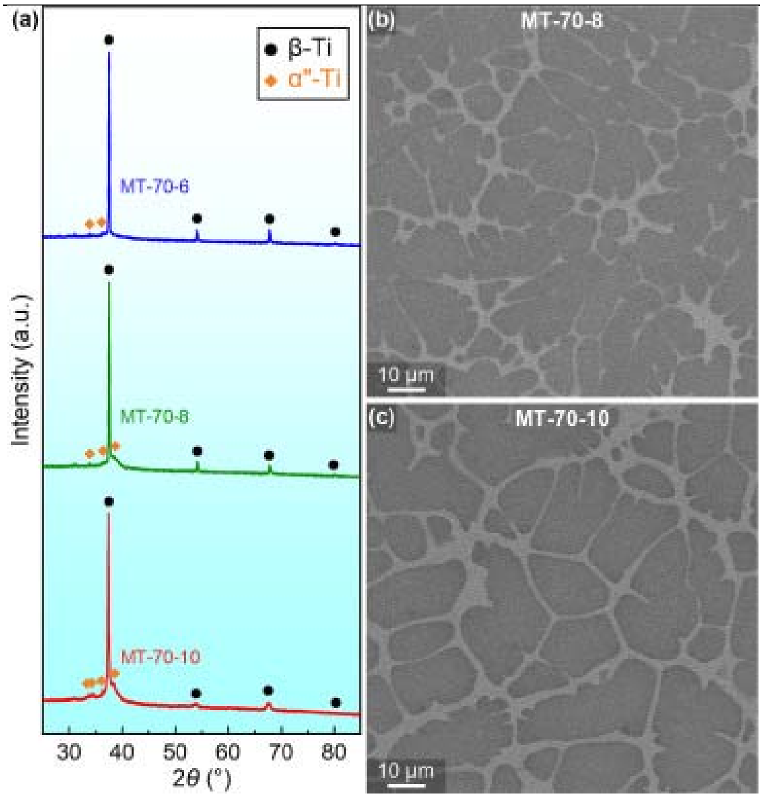

1. Download: Download high-res image (750KB)
2. Download: Download full-size image

Fig. 9. (a) XRD patterns of as-cast MT-70 plates with different thickness. (c) and (d) SEM micrographs of as-cast MT-70–8 and MT-70–10 BMGCs, respectively.

Fig. 10 shows the a_K and A_K of the MT-70 BMGCs fabricated under different cooling rates. At 298 K, a_K slightly increases from 24.8 ± 0.8 J cm^{-2} of MT-70–6 to 25.3 ± 0.5 J cm^{-2} of MT-70–8 and 26.3 ± 0.8 J cm^{-2} of MT-70–10, suggesting that a lower cooling rate results in a marginal increase in impact toughens of phase transformable BMGCs. However, a_K of the MT-70 BMGCs is more or less the same at 77 K, which marginally increases from 10.8 ± 1.0 J cm^{-2} of MT-70–6 to 11.0 ± 0.8 J cm^{-2} of MT-70–8 and 11.5 ± 1.0 J cm^{-2} of MT-70–10. The proctographic and microstructural features of the fractured MT-70–10 samples are selectively shown in Fig. S9. The cracking routes of MT-70–10 at both 298 and 77 K also exhibits tortuous routes with many crack deflections, similar to MT-70–6. A high density of martensitic plates and shear bands can be observed in the MT-70–10 fractured at 298 K, which with a low density can also be seen in the MT-70–10 sample tested at 77 K.

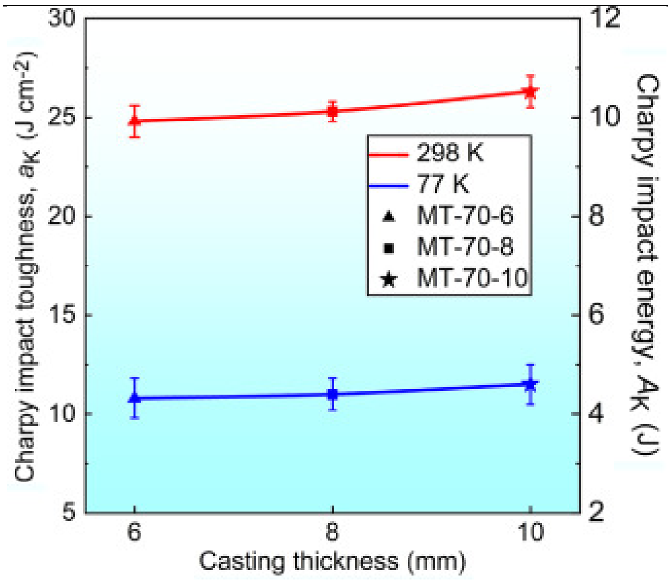

1. Download: Download high-res image (176KB)
2. Download: Download full-size image

Fig. 10. Charpy impact toughness, a_K, and impact energy, A_K, of MT-70 plates with different casting thickness at 298 and 77 K.

4. Discussion

4.1. Toughening BMGCs at low temperatures via DIMT of phase transformable crystals

It has been widely reported that the quasi-static and impact toughness' of BMGCs at room temperature are substantially higher than the respective properties of the monolithic BMGs [28,29,48,56,57]. However, a drastic reduction in the toughness of BMGCs with decreasing temperature can be expected, as both the glassy matrix and the BCC β-Zr/Ti crystals are susceptible to DBT at sub-ambient temperatures [27,36,37]. Such a variation is in accordance with their uniaxial tensile properties. BMGCs generally exhibit an increase in strength but severe deterioration of ductility at low temperatures [41,58]. A recent work reveals that BMGCs containing phase transformable crystals can exhibit simultaneously enhanced strength and tensile ductility with decreasing temperature [41,59]. These results imply that phase transformable BMGCs could possess higher toughness at low temperatures, and this scenario is substantiated by the results of the current work. As seen, a_K of NT-55, which contains β-Ti crystals that are not susceptible to stress-induced martensitic transformation and only plastically deform via dislocations, decreases precipitously, as shown in Fig. 2. In comparison, the toughness of MT-55 with β-Ti crystals that undergo DIMT increases—albeit marginally—first before decreasing. Importantly, it retains a high toughness even at 100 K.

For a quantitative comparison of a BMGC's ability to retain its toughness with decreasing temperature, the following dimensionless stability index, S, is used:

$$S = \frac{a_K(100\,K)}{a_K(298\,K) - a_K(100\,K)} \quad (2)$$

where a_K (298 K) and a_K (100 K) are the a_K values at 298 and 100 K, respectively. The choice of 100 K is made because the reported a_K values of many BMGs and BMGCs were obtained at that temperature (rather than 77 K) by considering a temperature rise of the small samples (3 × 3 × 30 mm) that are often for the a_K measurements [27,48]. It is clear from Eq. (2) that a higher a_K at 100 K and a smaller decrease in a_K from 298 to 100 K can lead to a higher S. One important caveat of using S is that its value has no significance when the material is inherently brittle. The values of a_K reported for different BMGs and BMGCs at 298 and 100 K as well as the calculated S values are listed in Table S1. The variation of a_K(100 K) with S is displayed in Fig. 11. The current NT-55 with stable β-Ti crystals exhibit similar a_K at 100 K and stability index as the previously reported BMGCs. However, MT-55 with phase transformable β-Ti crystals exhibits a much improved a_K of 12.3 J cm^{-2} at 100 K and an S value of 2.62, both of which are the highest, indicating that MT-55 possesses the best low-temperature toughness among all the BMGs and BMGCs developed so far.

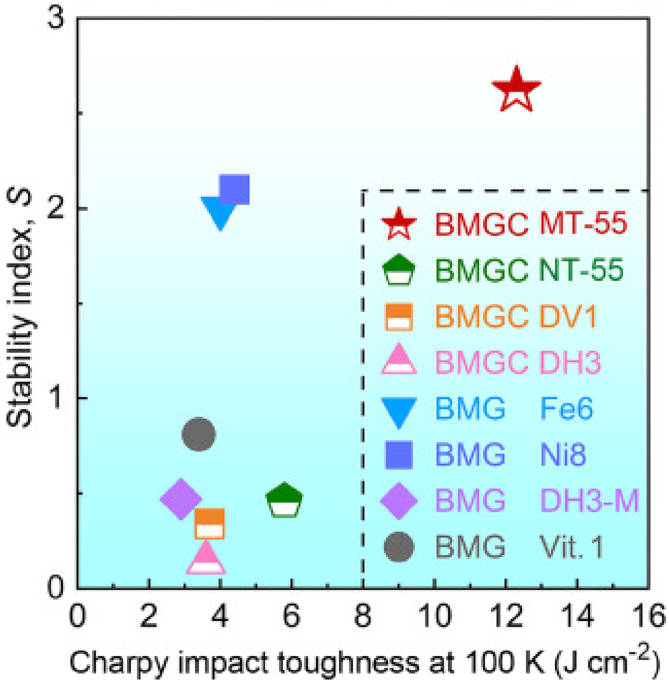

1. Download: Download high-res image (255KB)
2. Download: Download full-size image

Fig. 11. Comparison of a_K at 100 K and the stability index, *S*, of the reported BMGs [27,36] and BMGCs [27,48].

The superior low-temperature a_K of MT-55 is associated with the characteristics of phase transformable β-Ti crystals, as discussed below. Since DIMT takes place at a low critical stress, MT-55 shows relatively low yield strength of only ~780 MPa at 298 K, which is much smaller than BMGCs with stable β-Ti crystals [34,41]. The much lower yield strength of MT-55 causes a bit lower a_K of 17.0 J cm^{-2} than 18.5 J cm^{-2} of NT-55 at 298 K. However, contrast to the rapid toughness-reduction of NT-55, a_K of the MT-55 firstly increases as temperature decreasing from 298 to 240 K, which arises from the combination of characteristic properties of phase transformable crystals and the glassy matrix. Lower temperature readily promotes the DIMT of free-standing phase transformable crystals, which absorbs energies and benefits gross plasticity, known as the transformation-induced plasticity (TRIP) effect [33,60]. However, the phase transformable β-Ti crystals in MT-55 are confined by the glassy matrix. With decreasing temperature, the strength of metallic glasses increases, which exerts a stronger confining of DIMT of crystals, but the confining effect is largely relieved as shear bands forms which soften the glassy matrix [41]. Therefore, with decreasing the temperature, phase transformable BMGCs can exhibit simultaneous enhancement of strength and tensile ductility. Such a mechanism arising from the characteristic properties of both phases also accounts for the enhanced toughness of MT-55 from 298 to 240 K. It is noteworthy that MT-55 exhibits a simultaneous enhancement of strength and ductility as temperature decreasing down to 143 K, which is ~100 K lower than 240 K. The reason for the maximum toughness of MT-55 at 240 K is because only the narrow adjacent regions near the notch and alongside the cracking route undergo plasticity deformation and DIMT of β-Ti crystals during impact, which is very different with the case of uniform tensile deformation [37]. The DIMT of β-Ti crystals in MT-55 induces the formation of more shear bands in the glass matrix and also hardens the crystals, which causes the large plastic regions alongside the cracks, tortuous cracking routes and rugged fracture surfaces. In addition, the DIMT of β-Ti crystals absorb loading energy itself [45,61]. All these factors work together to partially compensate the brittleness of the glassy matrix as temperature further decreasing from 240 K down to 100 K, causing the slow decrease of a_K of the MT-55. This steady decrease in a_K with decreasing temperatures in MT-55 is attributed to the variations in the ease of occurrence of DIMT in the β-Ti dendrites. DIMT accommodates plastic deformation and absorbs energy during impact, which implies that its increased occurrence will significantly enhance the impact toughness of these BMGCs. In a recent study, some of the authors of this study studied the deformation behavior of MT-55 at different temperatures. It was observed that the DIMT of the β-Ti dendrites is suppressed at temperatures < 100 K [41]. This suppression of DIMT is attributed to a greater plastic constraint imposed by the amorphous matrix on the dendrites, specifically at low temperatures. Note that DIMT of dendrites during plastic deformation accommodates large shear strains and the subsequent slip transfer to the amorphous matrix leads to profuse shear banding in the latter. However, at low temperatures, the stress required to operate STZs in the amorphous phase increases with decreasing temperatures [49]. This implies that the slip transfer from dendrites to the amorphous matrix will occur at significantly higher stresses. As a result, the strain in the dendrites is suppressed, which in turn mitigates DIMT. In fact, the reduced fraction of α″-Ti observed in β- dendrites at 77 K than that at RT is an outcome of this effect. As a result, limited plasticity is observed in MT-55 at low temperatures, which also manifests as a steady decrease in a_K. Nevertheless, a_K of the MT-55 is much higher than NT-55 at low temperatures, which implies that the BMGCs can be toughened by DIMT of phase transformable crystals, substantiating the longstanding conjecture in the community. Several studies have suggested that the plasticity of BMGs can be significantly improved by performing cyclic cryogenic treatment (CCT), also referred to as rejuvenation [62], [63], [64], [65], [66]. This treatment helps in enhancing the plasticity of the BMG by introducing a non-affine strain at the atomic scale. It is then worth considering if performing CCT on the BMGCs chosen in this study will rejuvenate the BMG matrices and further enhance its impact toughness. It has been reported that significant enhancement in plasticity, which directly correlates with a_K, can be observed for different BMGs when they are subjected to CCT. However, they explicitly mentioned that the degree and effectiveness of rejuvenation is sensitive to the thermal history and composition of the material [[62], [63], [64],67]. In another study, Rajpoot et al. measured the fracture toughness of as cast and rejuvenated BMGCs, one with transforming and the other with non-transforming dendrites, after subjecting them to CCT [29]. It was observed that the fracture toughness of the rejuvenated BMGCs is similar to that of their as cast counterpart although their plasticity significantly. This suggests that the rejuvenation treatment may not necessarily be effective in the context of improving fracture toughness or impact toughness. While it is possible that the CCT will enhance the fracture toughness and impact toughness of certain other BMGC compositions, perhaps incrementally, further investigations are required before making any definitive statements in this regard.

4.2. Enhancing the impact toughness of BMGCs via microstructural optimization

The Charpy impact tests of the MT-*X* BMGCs reveals that the toughness is strongly associated with microstructures. With increasing the fraction of the phase transformable β-Ti crystals from MT-25 to MT-75, a_K at both 298 and 77 K monotonically increases, but which largely decreases from MT-70 to the fully crystalline MT-100, suggesting that a_K of the phase transformable MT-55 can be further enhanced via microstructural optimization. MT-70 possesses the highest a_K of 24.8 ± 0.8 J cm^{-2} at 298 K and 10.8 ± 1.0 J cm^{-2} at 77 K. The previously-reported a_K of monolithic BMGs [36,[68], [69], [70]] and BMGCs [22,27,48,71,72] at 298 K and cryogenic temperatures (77–100 K) are listed in Table S2 and Table S3, respectively. These data together with the a_K of the current BMGCs are displayed in Fig. 12. At 298 K, except the Zr-based DH3 BMGC with a high fraction of stable crystals, the a_K of the MT-70 BMGCs exceeds all the other BMGs and BMGCs reported so far, as seen in Fig. 12(a). It is noteworthy that the size of the DH3 specimens used for the impact tests is only 3 × 3 × 30 mm^3, much smaller than the sample size (5 × 10 × 55 mm^3) used for the current testing. A smaller sample size generally results in a higher measured a_K [36,48,51,73]. At 77 K, the current MT-70 BMGCs with phase transformable β-Ti crystals exhibit a much superior a_K (more than three times higher) than all the reported BMGs and BMGCs (including DH3), as shown in Fig. 12(b).

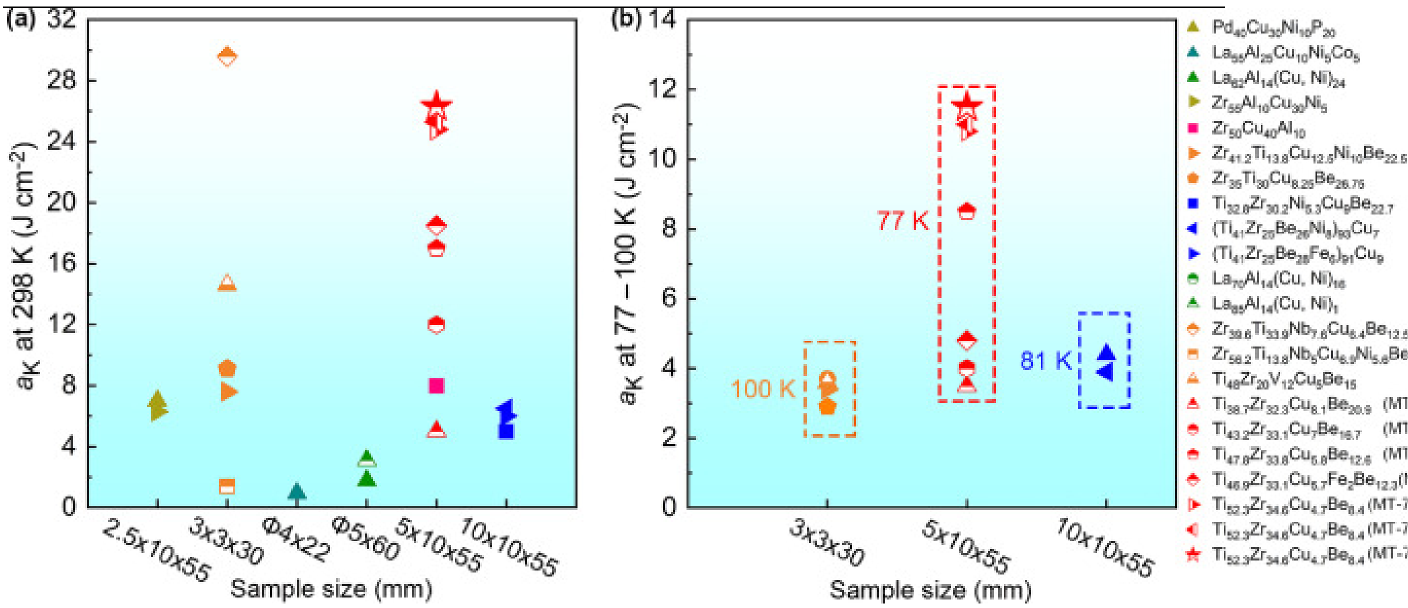

1. Download: Download high-res image (487KB)
2. Download: Download full-size image

Fig. 12. Comparison of a_K (a) at 298 K and (b) at 77 –100 K of the reported BMGs [36,[68], [69], [70]] and BMGCs [22,27,48,71,72].

The superior a_K of the MT-70 is the outcome of its optimized microstructure. As compared to MT-55, the volume fraction of β-Ti crystals in MT-70 is much higher, and therefore, a much higher amount of DIMT of phase transformable β-Ti crystals takes place in it during impact. This causes the larger plastic regions, much more tortuous cracking route and much rougher fractured surfaces of MT-70, benefiting the enhanced a_K. In addition, the glassy ligaments surrounding β-Ti crystals are much thinner in MT-70 as compared to MT-50, which means the confining of DIMT by the glassy matrix at low temperatures is much weaker. Therefore, more DIMT of β-Ti crystals at low temperatures leads to a high a_K of MT-70 even at 77 K. Such fundamental mechanisms also explain the microstructural dependence of a_K of other MT-*X* BMGCs. However, as the designed fraction of β-Ti increases to 100%, MT-100 exhibits a fully crystalline α″-Ti structure rather than β-Ti. This is because the supercooled liquid exerts a negentropic stabilizing effect on metastable β-Ti crystals to prevent the transformation to α′/α″-Ti during solidification of BMGCs [55]. MT-100 fully crystallizes into β-Ti crystals at high temperatures, then β-Ti crystals fully transform into α″-Ti without the negentropic stabilization by the supercooled liquid phase. MT-100 exhibits a low a_K, because the fully crystalline α″-Ti are stable at RT, which cannot undergo DIMT. Furthermore, the strength of full crystalline MT-100 is relatively low due to the absence of a glassy matrix, which additionally leads to the low a_K of MT-100.

4.3. Overcoming relaxation-induced brittleness of large-sized phase transformable BMGCs

Different to crystalline alloys, the structures and energy states of BMGs are closely dependent on cooling rates [29,64,74]. Under a lower cooling rate, the supercooled liquids evolve towards more equilibrium states, and BMGs with more relaxed and lower energy states are the outcome [74]. Recent tests show that the toughness of BMGs are sensitive to the energy states, and a smaller enthalpy of relaxation, which is the indicator of a lower energy state, causes an tremendous drop in toughness, known as the relaxation-induced brittleness [29,64]. Consequently, BMGs fabricated at lower cooling rates, show largely reduced toughness, which severely restricts the applications of large-sized parts of BMGs and BMGCs.

The relaxation enthalpies of the as-cast MT-70 plates with a thickness of 6 mm, 8 mm and 10 mm were measured, as shown in Fig. S8, which continuously decreases from 10.77 ± 0.53 J g^{-1} of MT-70–6 to 10.29 ± 0.36 J g^{-1} of MT-70–8 and 9.84 ± 0.41 J g^{-1} of MT-70–10, indicating a more relaxed state of the glassy matrix. Therefore, a_K of the MT-70 plates was expected to decrease with increasing the casting thickness. However, as shown in Fig. 10 and listed in Table 2, a_K of the MT-70 increases with decreasing cooling rates. The volume fractions and compositions of β-Ti crystals in the three MT-70 BMGCs are detected almost identical due to its quasi-equilibrium nature, but the average β-Ti crystal size monotonically increases from 7.2 ± 1.9 μm in MT-70–6 to 8.6 ± 1.6 μm in MT-70–8 and 10.1 ± 1.8 μm in MT-70–10. It has been widely reported that it is easier for larger crystals to undergo DIMT due to a large reduction of Gibbs free energy (driving force) and a low stored elastic energy (hindrance) [33,42,45]. Therefore, a higher amount of DIMT of the β-Ti crystals takes place in the BMGCs obtained at lower cooling rates, which contributes to a higher a_K and can sufficiently overcompensate the brittleness of the glassy matrix. Consequently, although the glassy matrix undergoes relaxation-induced brittleness, the phase transformable BMGCs can exhibit enhanced toughness with increasing casting size, as confirmed in the current MT-70 plates. Before closing, we would like to address the relatively higher enhancement in a_K of MT-70 BMGCs at 298 K than at 77 K. The cooling rates of any material undergoing solidification is a function of its casting size. Note that the cooling rates are inherently lower in large castings compared to that in smaller castings. Owing to this, the dendrites in larger castings of MT-70 BMGCs have sufficient time to coarsen, but those in smaller ones do not. Prior studies have shown that the occurrence of DIMT is sensitive to the crystallite size; i.e. more DIMT occurs in larger crystallites and vice versa [33,45]. Since the increased occurrence of DIMT enhances the plasticity as well as the impact toughness of BMGCs, larger castings of MT-70 exhibit a more pronounced increase in impact toughness at 298 K. Alternately, since a plastic constraint is imposed by the BMG matrix on the dendrites at lower temperatures (<100 K), the occurrence of DIMT in them is limited (see Section 4.2). Therefore, the decreased occurrence of DIMT in dendrites of MT-70 at 77 K, limits its plastic deformation and diminishes the enhancement in impact toughness compared to that observed at 298 K.

5. Conclusions

The Charpy impact toughness, a_K, of Ti-based BMGCs reinforced with β-Ti crystalline dendrites with different phase stability, volume fraction and size were investigated. The primary findings of this study are summarized below:

- The a_K of the NT-55 BMGC with stable β-Ti crystals monotonically decreases with decreasing temperature, but that of MT-55 BMGC with phase transformable β-Ti crystals initially increases as temperature decreases from 298 to 240 K, then gradually decreases with further reduction in temperature. The difference in the variations of a_K is attributed to the deformability of the transformable β-Ti crystals over a wide range of temperature, which absorbs the impact energy by undergoing deformation-induced martensitic transformation (DIMT). The a_K of MT-55 at 100 K is the highest amongst that of BMGs and BMGCs examined so far.
- On increasing the mole fraction of phase transformable β-Ti crystals from 25% to 70%, a_K at both 298 and 77 K monotonically increases. Increasing the mole fraction of β-Ti crystals increases the crystallite size, which in turn, improves its transformability. Also, as the fraction of the BMG matrix reduces, its constraining effect on the dendrites diminishes, which also promotes DIMT at lower stresses. This suggests that enhancement in a_K via microstructural optimization of the transformable β-Ti in BMGCs is possible. However, when the mole fraction of β-Ti is 100%, it fully transforms to an α″-Ti alloy. Since DIMT is unlikely to further occur in this alloy, it has a much lower a_K than that of BMGCs containing 55% and 70% mole fraction of dendrites.
- The slower cooling rates in larger castings generally causes relaxation-induced brittleness of BMGs and BMGCs. However, the MT-70 plates with larger casting thickness exhibit marginally higher a_K at both 298 and 77 K than smaller ones, as the lower cooling rate in the former increases the size of β-Ti crystals. This enhances the ability of the dendrites in larger castings of BMGCs to undergo DIMT, which in turn, leads to their enhanced a_K. Therefore, such BMGCs are resistant to relaxation-induced embrittlement.

These findings provide a guideline for designing large-sized BMGCs that have high impact toughness at both ambient and sub-ambient temperatures.

Declaration of Competing Interest

The authors declare that they have no known competing financial interests or personal relationships that could have appeared to influence the work reported in this paper.

Acknowledgments

This work is supported by the National Natural Science Foundation of China (Nos. 52171164 and 51790484), the National Key Research and Development Program of China (2021YFA0716303 and 2018YFB0703402), Start-up research grant (No. SRG/2020/000095) of Science and Engineering Research Board, DST, GoI, A*STAR, Singapore via the Structural Metals and Alloys Programme (No. A18B1b0061), the Natural Science Foundation of Liaoning Province (2021-MS-009), the China Manned

Space Engineering, the Chinese Academy of Sciences (ZDBS-LY-JSC023), and the Youth Innovation Promotion Association CAS (2021188).

Appendix. Supplementary materials

Download: Download Acrobat PDF file (2MB)

References

[1]

C. Schuh, T. Hufnagel, U. Ramamurty

Mechanical behavior of amorphous alloys

Acta Mater, 55 (12) (2007), pp. 4067-4109

View PDFView articleView in ScopusGoogle Scholar
[2]

W.H. Wang

Dynamic relaxations and relaxation-property relationships in metallic glasses

Prog. Mater. Sci., 106 (2019), Article 100561

View PDFView articleView in ScopusGoogle Scholar
[3]

T.C. Hufnagel, C.A. Schuh, M.L. Falk

Deformation of metallic glasses: recent developments in theory, simulations, and experiments

Acta Mater., 109 (2016), pp. 375-393

View PDFView articleView in ScopusGoogle Scholar
[4]

A.L. Greer, Y.Q. Cheng, E. Ma

Shear bands in metallic glasses

Mater. Sci. Eng. R, 74 (4) (2013), pp. 71-132

View PDFView articleView in ScopusGoogle Scholar
[5]

R. Maaß, J.F. Löffler

Shear-band dynamics in metallic glasses

Adv. Funct. Mater., 25 (16) (2015), pp. 2353-2368

CrossrefView in ScopusGoogle Scholar
[6]

T. Rouxel, J.-i. Jang, U. Ramamurty

Indentation of glasses

Prog. Mater. Sci., 121 (2021), Article 100834

View PDFView articleView in ScopusGoogle Scholar
[7]

K. Kosiba, D. Şopu, S. Scudino, L. Zhang, J. Bednarcik, S. Pauly

Modulating heterogeneity and plasticity in bulk metallic glasses: role of interfaces on shear banding

Int. J. Plast, 119 (2019), pp. 156-170

View PDFView articleView in ScopusGoogle Scholar
[8]

A. Bhattacharyya, G. Singh, K.E. Prasad, R. Narasimhan, U. Ramamurty

On the strain rate sensitivity of plastic flow in metallic glasses

Mater. Sci. Eng. A, 625 (2015), pp. 245-251

View PDFView articleView in ScopusGoogle Scholar
[9]

M.Q. Jiang, G. Wilde, J.H. Chen, C.B. Qu, S.Y. Fu, F. Jiang, L.H. Dai

Cryogenic-temperature-induced transition from shear to dilatational failure in metallic glasses

Acta Mater, 77 (2014), pp. 248-257

View PDFView articleView in ScopusGoogle Scholar
[10]

J.J. Lewandowski, A.L. Greer

Temperature rise at shear bands in metallic glasses

Nat. Mater., 5 (1) (2006), pp. 15-18

CrossrefView in ScopusGoogle Scholar

[11]

B.A. Sun, W.H. Wang

The fracture of bulk metallic glasses

Prog. Mater. Sci., 74 (2015), pp. 211-307

View PDFView articleView in ScopusGoogle Scholar
[12]

J.C. Qiao, Q. Wang, J.M. Pelletier, H. Kato, R. Casalini, D. Crespo, E. Pin
eda, Y. Yao, Y. Yang

Structural heterogeneities and mechanical behavior of amorphous alloys

Prog. Mater. Sci., 104 (2019), pp. 250-329

View PDFView articleView in ScopusGoogle Scholar
[13]

L.Q. Shen, J.H. Yu, X.C. Tang, B.A. Sun, Y.H. Liu, H.Y. Bai, W.H. Wang

Observation of cavitation governing fracture in glasses

Sci. Adv., 7 (14) (2021), p. eabf7293

View in ScopusGoogle Scholar
[14]

D.C. Hofmann, J.Y. Suh, A. Wiest, M.L. Lind, M.D. Demetriou, W.L. Johns
on

Development of tough, low-density titanium-based bulk metallic glass matrix composites with tensile ductility

PNAS, 105 (51) (2008), pp. 20136-20140

CrossrefView in ScopusGoogle Scholar
[15]

D.C. Hofmann, J.Y. Suh, A. Wiest, G. Duan, M.L. Lind, M.D. Demetriou, W
.L. Johnson

Designing metallic glass matrix composites with high toughness and tensile ductility

Nature, 451 (7182) (2008), pp. 1085-1089

CrossrefView in ScopusGoogle Scholar
[16]

J. Qiao, H. Jia, P.K. Liaw

Metallic glass matrix composites

Mater. Sci. Eng. R, 100 (2016), pp. 1-69

View PDFView articleView in ScopusGoogle Scholar
[17]

S. Pauly, G. Liu, G. Wang, U. Kuhn, N. Mattern, J. Eckert

Microstructural heterogeneities governing the deformation of $Cu_{47.5}Zr_{47.5}Al_5$ bulk metallic glass composites
Acta Mater, 57 (18) (2009), pp. 5445-5453
View PDFView articleView in ScopusGoogle Scholar
[18]

L. Deng, L. Zhang, K. Kosiba, R. Limbach, L. Wondraczek, G. Wang, D. G u, U. Kühn, S. Pauly

CuZr-based bulk metallic glass and glass matrix composites fabricated by selective laser melting

J. Mater. Sci. Technol., 81 (2021), pp. 139-150

View PDFView articleGoogle Scholar
[19]

D. Sopu, X.D. Yuan, F. Moitzi, M. Stoica, J. Eckert

Structure-property relationships in shape memory metallic glass composites

Materials (Basel), 12 (9) (2019), p. 10

Google Scholar
[20]

W. Guo, M. Wang, Z. Qin, X. Shen, S. Lü, X. Chen, S. Wu

Improving the glass-forming ability and plasticity of a TiCu-based bulk metallic glass composite by minor Ta doping

J. Alloys Compd., 884 (2021), Article 161054

View PDFView articleView in ScopusGoogle Scholar
[21]

C.C. Hays, C.P. Kim, W.L. Johnson

Microstructure controlled shear band pattern formation and enhanced plasticity of bulk metallic glasses containing in situ formed ductile phase dendrite dispersions

Phys. Rev. Lett., 84 (13) (2000), pp. 2901-2904

View in ScopusGoogle Scholar
[22]

M.Q. Tang, H.F. Zhang, Z.W. Zhu, H.M. Fu, A.M. Wang, H. Li, Z.Q. Hu

TiZr-base bulk metallic glass with over 50mm in diameter

J. Mater. Sci. Technol., 26 (6) (2010), pp. 481-486

View PDFView articleView in ScopusGoogle Scholar
[23]

L. Zhang, S. Pauly, M. Tang, J. Eckert, H. Zhang

Two-phase quasi-equilibrium in β-type Ti-based bulk metallic glass composites

Sci. Rep., 6 (2016), p. 19235

View in ScopusGoogle Scholar
[24]

G. Lyu, J. Qiao, J.-.M. Pelletier, L. Zhang, H. Zhang, Y. Yao

Dynamic mechanical behaviors of a metastable β-type bulk metallic glass composite

J. Alloys Compd., 819 (2020), Article 153040

View PDFView articleView in ScopusGoogle Scholar
[25]

Y. Lu, S. Su, S. Zhang, Y. Huang, Z. Qin, X. Lu, W. Chen

Controllable additive manufacturing of gradient bulk metallic glass composite with high strength and tensile ductility

Acta Mater, 206 (2021), Article 116632

View PDFView articleView in ScopusGoogle Scholar
[26]

Y. Chen, C. Tang, J.-.Z. Jiang

Bulk metallic glass composites containing B2 phase

Prog. Mater. Sci., 121 (2021), Article 100799

View PDFView articleView in ScopusGoogle Scholar
[27]

S. Roberts, C. Zachrisson, H. Kozachkov, A. Ullah, A.A. Shapiro, W.L. Joh nson, D.C. Hofmann

Cryogenic Charpy impact testing of metallic glass matrix composites

Scripta Mater, 66 (5) (2012), pp. 284-287

View PDFView articleView in ScopusGoogle Scholar
[28]

M.E. Launey, D.C. Hofmann, J.-.Y. Suh, H. Kozachkov, W.L. Johnson, R. O. Ritchie

Fracture toughness and crack-resistance curve behavior in metallic glass-matrix composites

Appl. Phys. Lett., 94 (24) (2009), Article 241910

View in ScopusGoogle Scholar
[29]

D. Rajpoot, R.L. Narayan, L. Zhang, P. Kumar, H. Zhang, P. Tandaiya, U. Ramamurty

Fracture toughness of a rejuvenated β-Ti reinforced bulk metallic glass matrix composite

J. Mater. Sci. Technol., 106 (2022), pp. 225-235

View PDFView articleView in ScopusGoogle Scholar

[30]

D. Rajpoot, R.L. Narayan, L. Zhang, P. Kumar, H. Zhang, P. Tandaiya, U. Ramamurty

Shear fracture in bulk metallic glass composites

Acta Mater, 213 (2021), Article 116963

View PDFView articleView in ScopusGoogle Scholar
[31]

R.L. Narayan, P.S. Singh, D.C. Hofmann, N. Hutchinson, K.M. Flores, U. Ramamurty

On the microstructure-tensile property correlations in bulk metallic glass matrix composites with crystalline dendrites

Acta Mater, 60 (13–14) (2012), pp. 5089-5100

View PDFView articleView in ScopusGoogle Scholar
[32]

L. Zhang, H. Zhang, X. Ren, J. Eckert, Y. Wang, Z. Zhu, T. Gemming, S. Pauly

Amorphous martensite in β-Ti alloys

Nat. Commun., 9 (1) (2018), p. 506

Google Scholar
[33]

L. Zhang, R.L. Narayan, H.M. Fu, U. Ramamurty, W.R. Li, Y.D. Li, H.F. Zh ang

Tuning the microstructure and metastability of β-Ti for simultaneous enhancement of strength and ductility of Ti-based bulk metallic glass composites

Acta Mater, 168 (2019), pp. 24-36

View PDFView articleView in ScopusGoogle Scholar
[34]

J. Zhang, L. Zhang, H. Zhang, H. Fu, H. Li, H. Zhang

Strengthening Ti-based bulk metallic glass composites containing phase transformable β-Ti via Al addition

Scripta Mater, 173 (2019), pp. 11-15

View PDFView articleCrossrefGoogle Scholar
[35]

D. Raut, R.L. Narayan, P. Tandaiya, U. Ramamurty

Temperature-dependence of mode I fracture toughness of a bulk metallic glass

Acta Mater, 144 (2018), pp. 325-336

View PDFView articleView in ScopusGoogle Scholar
[36]

J.L. Gu, G.N. Yang, P. Gong, Y. Shao, K.F. Yao

Cryogenic charpy impact toughness of (Ti41Zr25Be26Ni8)93Cu7 bulk metallic glass

Mater. Sci. Eng. A, 786 (2020), Article 139442

View PDFView articleView in ScopusGoogle Scholar
[37]

J. Ketkaew, W. Chen, H. Wang, A. Datye, M. Fan, G. Pereira, U.D. Schwarz, Z. Liu, R. Yamada, W. Dmowski, M.D. Shattuck, C.S. O'Hern, T. Egami, E. Bouchbinder, J. Schroers

Mechanical glass transition revealed by the fracture toughness of metallic glasses

Nat. Commun., 9 (1) (2018), p. 3271

View in ScopusGoogle Scholar
[38]

R.L. Narayan, L. Tian, D. Zhang, M. Dao, Z.-.W. Shan, K.J. Hsia

Effects of notches on the deformation behavior of submicron sized metallic glasses: insights from in situ experiments

Acta Mater., 154 (2018), pp. 172-181

View PDFView articleView in ScopusGoogle Scholar

[39]

Y. Lu, Y.-.H. Zhang, E. Ma, W.-.Z. Han

Relative mobility of screw versus edge dislocations controls the ductile-to-brittle transition in metals

PNAS, 118 (37) (2021), Article e2110596118

View in ScopusGoogle Scholar
[40]

W. Chen, S. Cao, W. Kou, J. Zhang, Y. Wang, Y. Zha, Y. Pan, Q. Hu, Q. Sun, J. Sun

Origin of the ductile-to-brittle transition of metastable β-titanium alloys: self-hardening of ω-precipitates

Acta Mater. (2019)

Google Scholar
[41]

L. Zhang, J. Zhang, H. Ke, B. Sun, Z. Zhu, Y. Wang, H. Li, A. Wang, H. Zhang

On low-temperature strength and tensile ductility of bulk metallic glass composites containing stable or shape memory β-Ti crystals

Acta Mater., 222 (2022), Article 117444

View PDFView articleView in ScopusGoogle Scholar
[42]

Y.S. Oh, C.P. Kim, S. Lee, N.J. Kim

Microstructure and tensile properties of high-strength high-ductility Ti-based amorphous matrix composites containing ductile dendrites

Acta Mater., 59 (19) (2011), pp. 7277-7286

View PDFView articleView in ScopusGoogle Scholar
[43]

Z. Yu, W. Zheng, Z. Li, Y. Lu, X. Yun, Z. Qin, X. Lu

Accelerated exploration of TRIP metallic glass composite by laser additive manufacturing

J. Mater. Sci. Technol., 78 (2021), pp. 68-73

View PDFView articleView in ScopusGoogle Scholar
[44]

ASTM E23-18

Standard Test Methods for Notched Bar Impact Testing of Metallic Materials

ASTM International (2018)

https://www.astm.org/e0023-18.html
Google Scholar
[45]

S. Banerjee, P. Mukhopadhyay

Phase Transformations-Examples from Titanium and Zirconium alloys

Elsevier, Oxford, UK (2007)

Google Scholar
[46]

L. Zhang, S. Chen, H. Fu, H. Li, Z. Zhu, H. Zhang, Z. Li, A. Wang, H. Zhang

Tailoring modulus and hardness of in-situ formed β-Ti in bulk metallic glass composites by precipitation of isothermal ω-Ti

Mater. Des., 133 (2017), pp. 82-90

View PDFView articleView in ScopusGoogle Scholar
[47]

L. Zhang, R.L. Narayan, B.A. Sun, T.Y. Yan, U. Ramamurty, J. Eckert, H.F. Zhang

Cooperative shear in bulk metallic glass composites containing metastable β-Ti dendrites

Phys. Rev. Lett., 125 (5) (2020), Article 055501

View in ScopusGoogle Scholar
[48]

C. Zachrisson, H. Kozachkov, S. Roberts, G. Kaltenboeck, R.D. Conner, M.D. Demetriou, W.L. Johnson, D.C. Hofmann

Effect of processing on Charpy impact toughness of metallic glass matrix composites

J. Mater. Res., 26 (10) (2011), pp. 1260-1268

CrossrefView in ScopusGoogle Scholar
[49]

C. Wang, Q.P. Cao, X.D. Wang, D.X. Zhang, U. Ramamurty, R.L. Narayan, J.Z. Jiang

Intermediate temperature brittleness in metallic glasses

Adv. Mater., 29 (14) (2017), p. 5

Google Scholar
[50]

B. Gludovatz, A. Hohenwarter, D. Catoor, E.H. Chang, E.P. George, R.O. Ritchie

A fracture-resistant high-entropy alloy for cryogenic applications

Science, 345 (6201) (2014), pp. 1153-1158

CrossrefView in ScopusGoogle Scholar
[51]

B. Gludovatz, D. Granata, K.V.S. Thurston, J.F. Löffler, R.O. Ritchie

On the understanding of the effects of sample size on the variability in fracture toughness of bulk metallic glasses

Acta Mater, 126 (2017), pp. 494-506

View PDFView articleView in ScopusGoogle Scholar
[52]

D.H. Ping, Y. Yamabe-Mitarai, C.Y. Cui, F.X. Yin, M.A. Choudhry

Stress-induced α″ martensitic (110) twinning in β-Ti alloys

Appl. Phys. Lett., 93 (15) (2008), Article 151911

View in ScopusGoogle Scholar
[53]

Y.W. Chai, H.Y. Kim, H. Hosoda, S. Miyazaki

Self-accommodation in Ti–Nb shape memory alloys

Acta Mater., 57 (14) (2009), pp. 4054-4064

View PDFView articleView in ScopusGoogle Scholar
[54]

X.H. Lin, W.L. Johnson

Formation of Ti-Zr-Cu-Ni bulk metallic glasses

J. Appl. Phys., 78 (11) (1995), pp. 6514-6519

View in ScopusGoogle Scholar
[55]

L. Zhang, H. Zhang, W. Li, T. Gemming, Z. Zhu, H. Fu, J. Eckert, S. Pauly

Negentropic stabilization of metastable β-Ti in bulk metallic glass composites

Scr. Mater., 125 (2016), pp. 19-23

View PDFView articleView in ScopusGoogle Scholar
[56]

P. Zhang, C. Zhang, D. Ouyang, L. Liu

Enhancement of plasticity and toughness of 3D printed binary $Zr_{50}Cu_{50}$ bulk metallic glass composite by deformation-induced martensitic transformation
Scr. Mater., 192 (2021), pp. 7-12
View PDFView articleView in ScopusGoogle Scholar
[57]

R. Raghavan, V.V. Shastry, A. Kumar, T. Jayakumar, U. Ramamurty

Toughness of as-cast and partially crystallized composites of a bulk metallic glass

Intermetallics, 17 (10) (2009), pp. 835-839

View PDFView articleView in ScopusGoogle Scholar
[58]

H.Y. Li, Z. Wang, H.J. Yang, X.H. Shi, J.W. Qiao, H.P. Zhang, Y.C. Wu

Work hardening and homogeneous elongation in metallic glass matrix composite at cryogenic temperature

Intermetallics, 126 (2020), Article 106877

View PDFView articleView in ScopusGoogle Scholar
[59]

S. Jiang, Y. Huang, P. Xue, F. Guo, Y. Ren, J. Sun, A.H.W. Ngan

Temperature-dependent deformation behavior of a CuZr-based bulk metallic glass composite

J. Alloys Compd., 858 (2021), Article 158368

View PDFView articleView in ScopusGoogle Scholar
[60]

Y. Wu, D. Ma, Q.K. Li, A.D. Stoica, W.L. Song, H. Wang, X.J. Liu, G.M. Stoica, G.Y. Wang, K. An, X.L. Wang, M. Li, Z.P. Lu

Transformation-induced plasticity in bulk metallic glass composites evidenced by in-situ neutron diffraction

Acta Mater., 124 (2017), pp. 478-488

View PDFView articleView in ScopusGoogle Scholar
[61]

H.Y. Kim, Y. Ikehara, J.I. Kim, H. Hosoda, S. Miyazaki

Martensitic transformation, shape memory effect and superelasticity of Ti–Nb binary alloys

Acta Mater., 54 (9) (2006), pp. 2419-2429

View PDFView articleView in ScopusGoogle Scholar
[62]

S.V. Ketov, Y.H. Sun, S. Nachum, Z. Lu, A. Checchi, A.R. Beraldin, H.Y. Bai, W.H. Wang, D.V. Louzguine-Luzgin, M.A. Carpenter, A.L. Greer

Rejuvenation of metallic glasses by non-affine thermal strain

Nature, 524 (7564) (2015), pp. 200-203

CrossrefView in ScopusGoogle Scholar
[63]

J. Ketkaew, R. Yamada, H. Wang, D. Kuldinow, B.S. Schroers, W. Dmowski, T. Egami, J. Schroers

The effect of thermal cycling on the fracture toughness of metallic glasses

Acta Mater., 184 (2020), pp. 100-108

View PDFView articleView in ScopusGoogle Scholar
[64]

B.S. Li, S. Xie, J.J. Kruzic

Toughness enhancement and heterogeneous softening of a cryogenically cycled Zr–Cu–Ni–Al–Nb bulk metallic glass

Acta Mater., 176 (2019), pp. 278-288

View PDFView articleView in ScopusGoogle Scholar
[65]

P. Gong, G. Yin, Z. Jamili-Shirvan, H. Ding, X. Wang, J. Jin

Influence of deep cryogenic cycling on the rejuvenation and plasticization of TiZrHfBeCu high-entropy bulk metallic glass

Mater. Sci. Eng. A, 797 (2020), Article 140078

View PDFView articleView in ScopusGoogle Scholar
[66]

Y. Du, W. Han, Q. Zhou, Y. Xu, H. Zhai, V. Bhardwaj, H. Wang

Enhancing the plasticity of a Ti-based bulk metallic glass composite by cryogenic cycling treatments

J. Alloys Compd., 835 (2020), Article 155247

View PDFView articleView in ScopusGoogle Scholar
[67]

J. Dong, Y. Huan, B. Huang, J. Yi, Y.H. Liu, B.A. Sun, W.H. Wang, H.Y. Bai

Unusually thick shear-softening surface of micrometer-size metallic glasses

The Innovation, 2 (2) (2021), Article 100106

View PDFView articleView in ScopusGoogle Scholar
[68]

Y. Yokoyama, N. Nishiyama, K. Fukaura, H. Sunada, A. Inoue

Rotating-beam fatigue strength of Pd40Cu30Ni10P20 bulk amorphous alloy

Mater. Trans., 40 (7) (1999), pp. 696-699

CrossrefView in ScopusGoogle Scholar
[69]

Y. Yokoyama, Y. Akeno, T. Yamasaki, P.K. Liaw, R.A. Buchanan, A. Inou e

Evolution of mechanical properties of cast $Zr_{50}Cu_{40}Al_{10}$ glassy alloys by structural relaxation
Mater. Trans., 46 (12) (2005), pp. 2755-2761
CrossrefView in ScopusGoogle Scholar
[70]

A. Inoue, T. Zhang

Impact fracture energy of bulk amorphous $Zr_{55}Al_{10}Cu_{30}Ni_{5}$ alloy
Mater. Trans., 37 (11) (1996), pp. 1726-1729
CrossrefView in ScopusGoogle Scholar
[71]

N. Nagendra, U. Ramamurty, T.T. Goh, Y. Li

Effect of crystallinity on the impact toughness of a La-based bulk metallic glass

Acta Mater, 48 (10) (2000), pp. 2603-2615

View PDFView articleView in ScopusGoogle Scholar
[72]

M.L. Lee, Y. Li, C.A. Schuh

Effect of a controlled volume fraction of dendritic phases on tensile and compressive ductility in La-based metallic glass

Acta Mater., 52 (14) (2004), pp. 4121-4131

View PDFView articleView in ScopusGoogle Scholar
[73]

R.L. Narayan, D. Raut, U. Ramamurty

A quantitative connection between shear band mediated plasticity and fracture initiation toughness of metallic glasses

Acta Mater, 150 (2018), pp. 69-77

View PDFView articleView in ScopusGoogle Scholar
[74]

Y. Sun, A. Concustell, A.L. Greer

Thermomechanical processing of metallic glasses: extending the range of the glassy state

Nat. Rev. Mater., 1 (2016), p. 16039

View in ScopusGoogle Scholar
[75]

L. Zhang, W. Li, Z. Zhu, H. Fu, H. Li, Z. Li, H. Zhang, A. Wang, H. Zhang

Distribution of Be in a Ti-based bulk metallic glass composite containing β-Ti

J. Mater. Sci. Technol., 33 (7) (2017), pp. 708-711

View PDFView articleView in ScopusGoogle Scholar